CHEMISTRY OF MATERIALS

Article

pubs.acs.org/cm

Light Hydrocarbon Adsorption Mechanisms in Two Calcium-Based Microporous Metal Organic Frameworks

Anna M. Plonka,[*,†,▽] Xianyin Chen,[‡] Hao Wang,[§] Rajamani Krishna,[*,∥] Xinglong Dong,[⊥] Debasis Banerjee,[§,○] William R. Woerner,[†] Yu Han,[⊥] Jing Li,[*,§] and John B. Parise[†,‡,#]

[†]Department of Geosciences, Stony Brook University, Stony Brook, New York 11794, United States

[‡]Department of Chemistry, Stony Brook University, Stony Brook, New York 11794, United States

[§]Department of Chemistry and Chemical Biology, Rutgers University, Piscataway, New Jersey 08854, United States

[∥]Van't Hoff Institute for Molecular Sciences, University of Amsterdam, Science Park 904, 1098 XH Amsterdam, The Netherlands

[⊥]King Abdullah University of Science and Technology, Thuwal 23955-6900, Kingdom of Saudi Arabia

[#]Photon Sciences, Brookhaven National Laboratory, Upton, New York 11973, United States

Supporting Information

ABSTRACT: The adsorption mechanism of ethane, ethylene, and acetylene (C_2H_n; n = 2, 4, 6) on two microporous metal organic frameworks (MOFs) is described here that is consistent with observations from single crystal and powder X-ray diffraction, calorimetric measurements, and gas adsorption isotherm measurements. Two calcium-based MOFs, designated as SBMOF-1 and SBMOF-2 (SB: Stony Brook), form three-dimensional frameworks with one-dimensional open channels. As determined from single crystal diffraction experiments, channel geometries of both SBMOF-1 and SBMOF-2 provide multiple adsorption sites for hydrocarbon molecules through C−H···π and C−H···O interactions, similarly to interactions in the molecular and protein crystals. Both materials selectively adsorb C_2 hydrocarbon gases over methane as determined with IAST and breakthrough calculations as well as experimental breakthrough measurements, with C_2H_6/CH_4 selectivity as high as 74 in SBMOF-1.

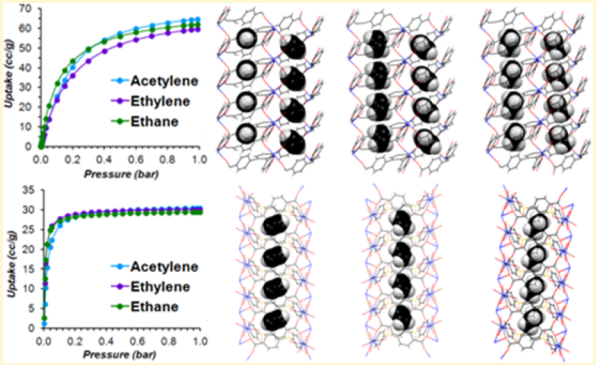

1. INTRODUCTION

For natural gas purification, CO_2 and light hydrocarbons are removed from methane in order to reduce CO_2-induced pipeline corrosion and produce high purity gases for energy and other industrial applications.[1] The purified methane obtained from natural gas is an alternative to gasoline or diesel automobile fuels.[2] Furthermore, natural gas is the main source of ethane, which is the second largest component after methane, ranging from 0.7 to 6.8 volume percent.[3] Ethane is the main feedstock for ethylene production, which in turn serves as the primary building block of polyethylene-based materials.[4] Thus, effective separation of light hydrocarbon gases (C_1−C_2) is important for the petroleum industry and influences the price and availability of plastics, used routinely in our daily lives. Currently, CO_2 and light hydrocarbon fractions of natural gas are separated through energy intensive cryogenic distillation; separation using solid state adsorbents capable of operating in higher temperatures is proposed as a more economical alternative.[5] Indeed several classes of porous solid state materials have been tested for industrially important gaseous hydrocarbon separation (e.g., C_2, C_3, C_4) with encouraging results.[6−8] Zeolites 5A and 13X can be used for the propylene/propane separation as reported by Järvelin and Fair.[6] Linear and branched hydrocarbon mixtures such as *n*-butane/*i*-butane or xylene isomers can be separated with MFI-type zeolites, with the reported separation factor between 20 and 60 for *n*-butane and over 600 for xylene.[7] Silver exchanged porous aromatic framework PAF-1-SO_3H effectively separates C_2 hydrocarbons, as reported by Ma and co-workers.[8]

Microporous MOFs, formed by metal atoms or atom clusters connected by organic ligands to form infinite networks, have sorption properties comparable or superior to benchmark solid state adsorbents.[9−13] MOFs possess seemingly limitless structural diversity, high flexibility, and in some cases easily modified frameworks that allow tuning for specific functions.[14,15] Possible industrial applications of MOFs include gas storage, gaseous and molecular separation, catalysis, or chemical sensing.[10,16−23] Selected MOF-based solid state adsorbents are utilized for various hydrocarbon separations.[5] For example, ZIF-7 and RPM-3-Zn [ZIF, zeolitic imidazole framework; $Zn(phim)_2$; phim, benzimidazole; RPM, Rutgers porous material; $Zn_2(bpdc)_2(bpee)$; bpdc, 4,4′-biphenyldicarboxylate;

Received: September 25, 2015
Revised: January 25, 2016
Published: January 25, 2016

DOI: 10.1021/acs.chemmater.5b03792
Chem. Mater. 2016, 28, 1636−1646

bpee, 1,2-bipyriylethylene] can separate C_2-C_4 hydrocarbons, due to the gate opening effect, happening at different pressures for smaller and larger molecules.[24,25] MOF-5 [$Zn_4O(bdc)_3$] separates methane from *n*-butane, and linear from branched alkanes.[26,27] HKUST-1 [HKUST, Hong Kong University of Science and Technology; $Cu_3(btc)_2$; btc, 1,3,5-benzenetricarboxylate] separates *o*-, *m*- and *p*-xylenes.[28]

Experimental gas adsorption studies of MOFs usually focus on gas isotherm measurments that, while providing the necessary information on the overall gas uptake and framework behavior upon gas loading, yield limited information on gas adsorption mechanism. Understanding the key atom−atom interactions responsible for high gas selectivity provides a means to discriminate between possible materials for industrial applications like natural gas purification. Long and co-workers recently reported the neutron diffraction study on C_2-C_3 hydrocarbon adsorption on Fe-MOF-74, which selectively adsorbs olefins over paraffins.[29] The selectivity originates in the stronger interaction between unsaturated than saturated hydrocarbons with bare Fe(II) sites, as determined from the distances between adsorbate and the open metal site.[29] Kitagawa and co-workers used *in situ* synchrotron powder X-ray diffraction (PXRD) techniques to discover the structural reasons for a high uptake of acetylene, and they located sorption sites in a small pore MOF, $Cu_2(pzdc)_2(pyz)$ (pzdc = pyrazine 2,3-dicarboxylate, pyz = pyrazine).[30] Further, MIL-47 [V(O)(bdc)] and MIL-53-Cr can separate xylene isomers, with MIL-47 displaying higher values of selectivity due to entropic effects.[31] The structure model of the xylene:MIL-47 adduct was determined by fitting it to synchrotron PXRD data with the Rietveld refinement technique.[31]

Single crystal X-ray diffraction has been used to characterize adsorption mechanisms of C_1-C_2 hydrocarbons in several MOFs, but only a very limited number of those studies are reported to date.[32] Kim and co-workers characterized the methane adsorption mechanism in $Zn_2(bdc)_2(dabco)$ [bdc = 1,4-benzenedicarboxylate, dabco = 1,4-diazabicyclo(2.2.2)-octane], as well as the acetylene adsorption on Mg and Mn formates.[33,34] The adsorption sites of various gases, including methane and acetylene in a $Sc_2(bdc)_3$ framework, were reported by Miller et al.[35] Finally, Zhang and Chen reported acetylene and carbon dioxide adsorption mechanism in MAF-2 (MAF, metal azolate framework; Cu(etz); Hetz, 3,5-diethyl-1,2,4-triazole), with a maximum acetylene uptake some 40 times higher than that for acetylene in a gas cylinder at 1.0−1.5 bar, due to the optimal geometry of the framework pores.[36]

Among the diverse range of porous MOFs reported so far, those containing biocompatible metals like calcium and magnesium are of special interest. The low toxicity and Earth abundance of Ca- and Mg-based MOFs, relative to first-row transitional metals or lanthanide-metal-based MOF analogues, may be especially beneficial in potential industrial applications.[37−39] We have recently reported several calcium MOFs with interesting properties.[40−43] Herein, we report the hydrocarbon adsorption mechanism determined from single crystal X-ray diffraction on two calcium-based MOFs: SBMOF-1 [Ca(sdb); sdb, 4,4′-sulfonyldibenzoate] and a novel material SBMOF-2 [Ca(tcpb); tcpb, 1,2,4,5-tetrakis(4-carboxyphenyl)-benzene]. Their C_2/C_1 selectivity was determined from the ideal adsorbed solution theory (IAST) calculations, supported by transient breakthrough calculations.[44,45] Since the examples related to the C_2H_n−framework interaction determined by the single crystal diffraction method are scarce, the detailed structural insights gained here will help design further gas-selective solids of this type.

SBMOF-1 is a porous metal organic framework, with moderate surface area of 145 m^2/g and calculated porosity of 16% (PLATON).[40,46] After removal of solvent water, SBMOF-1 does not adsorb water from the air and remains crystalline after exposure to 75% relative humidity for at least 2 months of storage (Figure S1). Structurally, SBMOF-1 is composed of Ca metal centers, coordinated by oxygen atoms in octahedral configuration and v-shaped sdb organic linkers, forming diamond-shaped 1-D channels along the *b* direction (Figure 1).

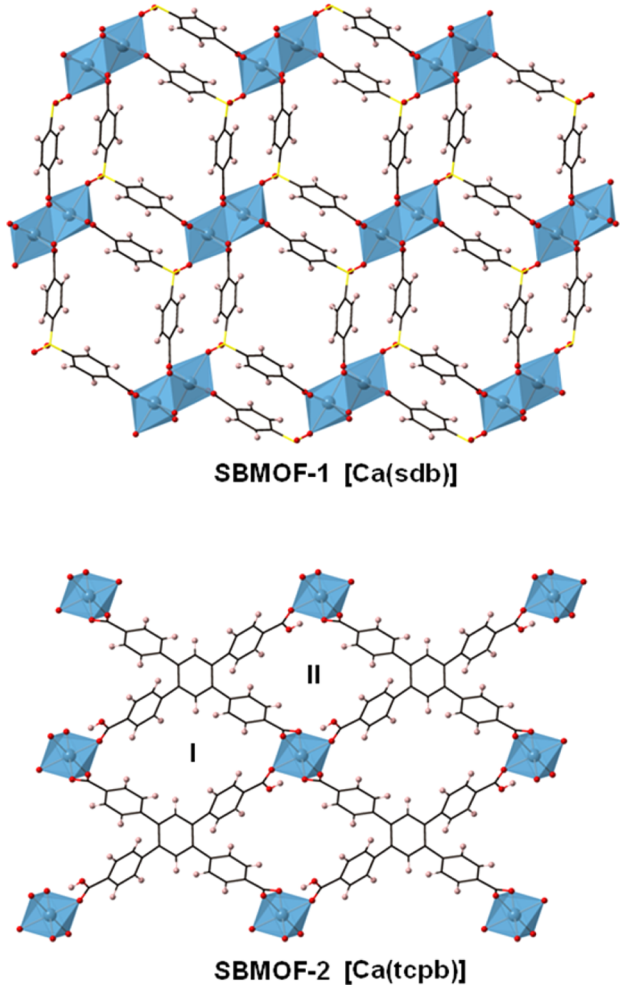

Figure 1. Polyhedral representation of the (a) SBMOF-1 and (b) SBOF-2 structures, as seen in [010] and [100], respectively. SBMOF-2 displays two crystallographically different types of channels, designated on the figure as I and II. Blue polyhedra represent Ca; red spheres, O; black wire, C; yellow wire, S; and pink spheres, H.

After removal of solvent water, the framework of SBMOF-1 undergoes a structural rearrangement involving the rotation of the sdb linker.[40] Our previous study showed that SBMOF-1 is selective toward CO_2 over N_2 and the selectivity arises from the geometry of the pores, where the CO_2 molecule interacts with two phenyl rings at a time through a quadrupole−π interaction.[47]

SBMOF-2 is a novel material that we recently reported, which shows high Xe/Kr selectivity of about 10 at 298 K and the surface area of 195 m^2/g, stable in both air and humidity (Figure S2).[43] Structurally it is based on isolated CaO_6

DOI: 10.1021/acs.chemmater.5b03792
Chem. Mater. 2016, 28, 1636−1646

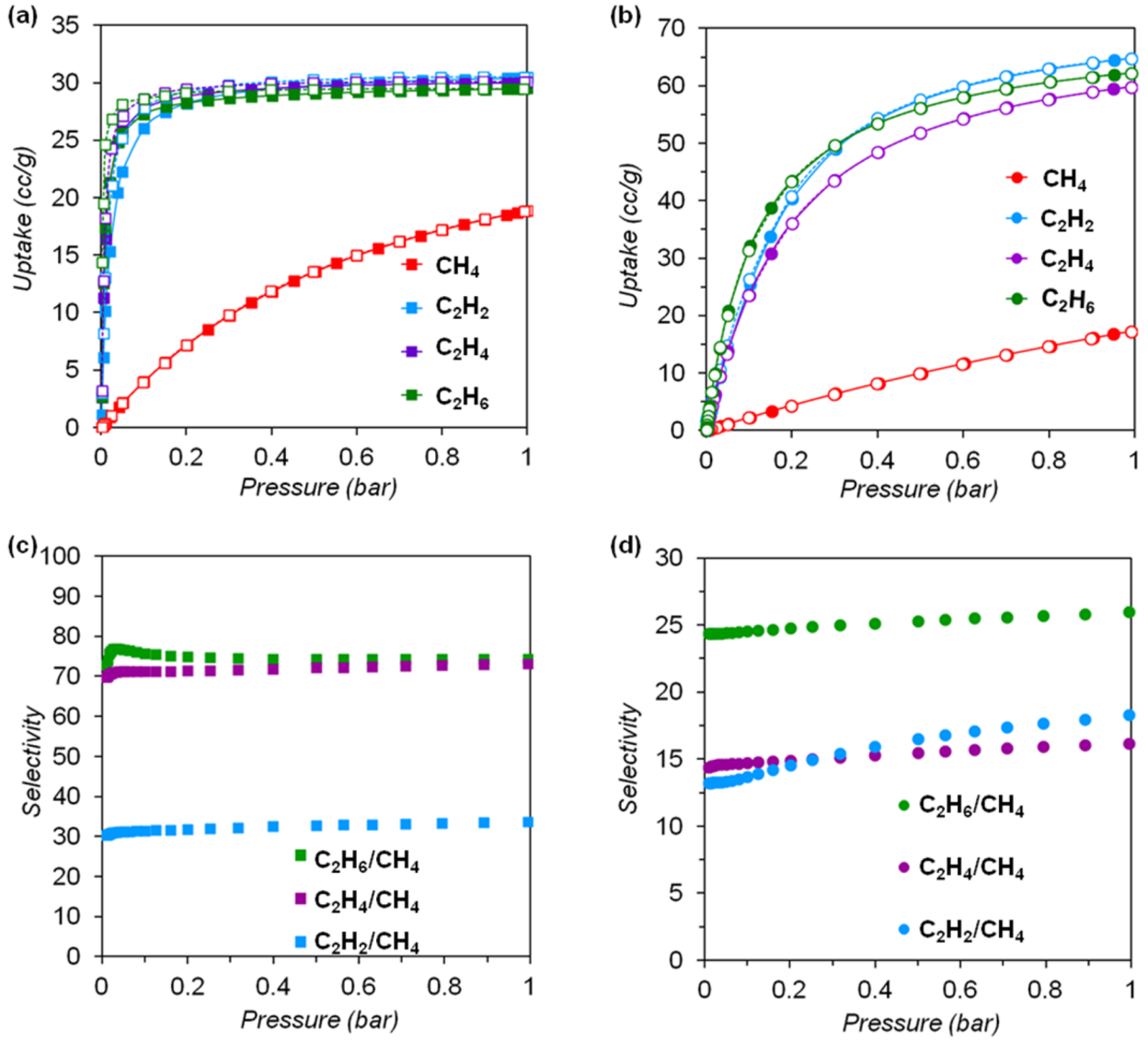

Figure 2. Gas adsorption isotherms of C_1−C_2 hydrocarbons at 298 K for (a) SBMOF-1 and (b) SBMOF-2; calculated C_2H_n/CH_4 selectivity at 298 K for (c) SBMOF-1 and (d) SBMOF-2.

octahedra, connected by a half-deprotonated tcpb linkers into a three-dimensional framework, with diamond-shaped channels running along *a* (Figure 1). SBMOF-2 has a permanent porosity of 25.6% (PLATON)[46] and contains two types of crystallographically different channels (types I and II).[43] The channels have walls built with phenyl rings, and additionally the channels of the type II contain polar −OH groups. Both the phenyl rings and oxygen atoms serve as strong adsorption sites for C_2H_n molecules. Similar to SBMOF-1, after removal of the native solvent water, SBMOF-2 does not saturate with the water vapor from the atmosphere as evident for thermogravimetric and diffraction experiments.[43]

2. EXPERIMENTAL SECTION

2.1. Synthesis and Sample Activation. SBMOF-1 and SBMOF-2 were synthesized according to the previously reported procedures under solvothermal conditions.[40,43] Starting materials include calcium chloride ($CaCl_2$, 96%, Acros-Organics), 1,2,4,5-tetrakis(4-carboxyphenyl)benzene acid [H_2(tcpb), 98%, Sigma-Aldrich], 4,4′-sulfonyldibenzoic acid [H_2(sdb), 98%, Sigma-Aldrich], and ethanol (95%, Fisher Scientific) and were used without further purification.

For the synthesis of SBMOF-1 a mixture of 0.074 g (0.6 mmol) of $CaCl_2$ and 0.198 g (0.6 mmol) of H_2sdb was dissolved in 10 g of ethanol and stirred for 3 h to achieve homogeneity. The solution was placed in an oven in 453 K and held at 453 K for 4 days. Products of the reaction were the colorless, prism-shaped crystals, which after recovering from the reaction were filtered and washed with ethanol (yield: ∼ 50%, 0.100 g).

For the synthesis of SBMOF-2 a mixture of 0.027 g (0.25 mmol) of $CaCl_2$ and 0.03 g (0.05 mmol) of H_2(tcpb) was dissolved in 12 g of ethanol and stirred for 2 h to achieve homogeneity. The resultant solution was heated at 373 K for 3 days in the oven. Colorless prism-shaped crystals were recovered as a product and washed with ethanol. The yield was ∼50%, 0.02 g.

As-synthesized SBMOF-1 and SBMOF-2 contain uncoordinated, disordered water molecules inside the channels. Water molecules come from the 95% ethanol solvent and the adsorbed moisture on the $CaCl_2$ reactant. For the removal of the solvent (activation), SBMOF-1 and SBMOF-2 were heated to 563 and 513 K, respectively, and held in vacuum for 12 h.[40,43]

2.2. Gas Adsorption. SBMOF-1 and SBMOF-2 were tested for C_1−C_2 hydrocarbon gas adsorption at 273/278, 288, 298 K and pressures up to 1 bar (Figure 2, Figures S3−S13). Additionally, adsorption

DOI: 10.1021/acs.chemmater.5b03792
Chem. Mater. 2016, 28, 1636−1646

of propane, propylene, and *n*-butane was measured for SBMOF-2, and the results are shown in Figure 3a.

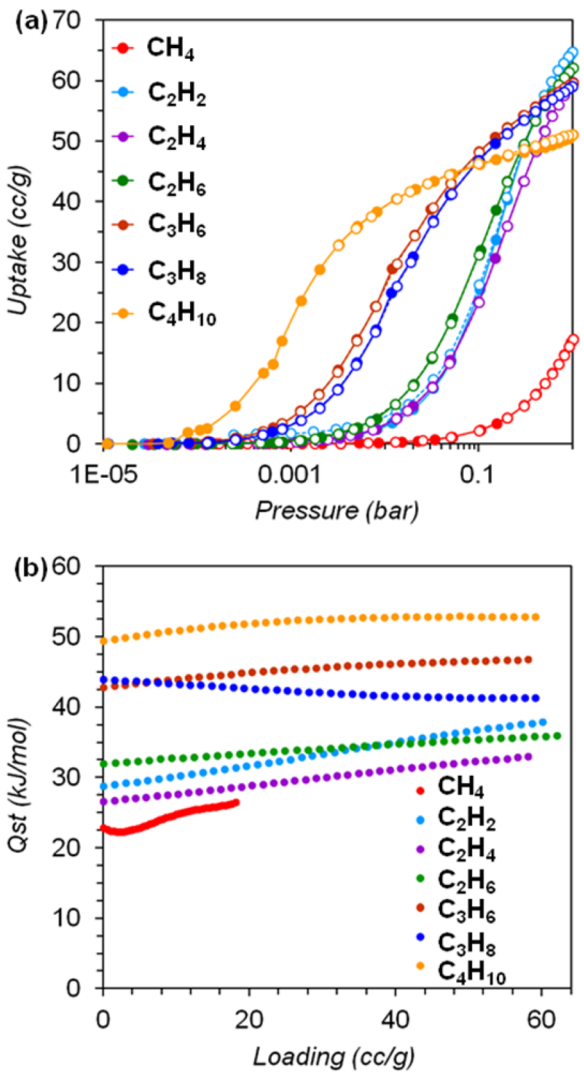

Figure 3. (a) Gas adsorption isotherms of C_1-nC_4 hydrocarbon gases at 298 K for SBMOF-2. (b) Isosteric heat of adsorption for C_1-nC_4 hydrocarbon gases on SBMOF-2 calculated with the virial method.

Gas adsorption studies of the materials described herein were performed with a volumetric gas sorption analyzer (Autosorb-1-MP, Quantachrome Instruments) with ultrahigh purity gases (99.999%). Initially, approximately 100 mg of the sample was activated under vacuum, for 12 h, and the weight was measured before and after activation to ensure the full solvent removal. After the system cooled, isotherms were collected at three different temperatures at pressures up to 1 bar. The activation step was repeated for the same sample between each run.

Single-component hydrocarbon adsorption isotherms were fitted with the DSLF model to enable the application of IAST in simulating the performance of SBMOF-1 and SBMOF-2 under a mixed-component gas (see Supporting Information).[44,48] The fitting parameters of the DSLF equation as well as the correlation coefficients (R^2) are listed in Table S1.Figures S14–S15 show experimental and fitted isotherms for C_1-C_2 hydrocarbon gases for SBMOF-1 and SBMOF-2 at 298 K.

2.3. Transient Breakthrough. We performed transient breakthrough simulations using the simulation methodology described in the literature.[45] For the breakthrough simulations, the following parameter values were used: length of packed bed, L = 0.3 m; voidage of packed bed, ε = 0.4; superficial gas velocity at inlet, u = 0.04 m/s. The simulation results for transient breakthrough are presented in terms of a dimensionless time τ, defined by dividing the actual time, t, by the characteristic time, $\frac{L\varepsilon}{\tau}$.

The supplementary breakthrough experiment was conducted using a lab-scale fix-bed reactor at 296 K. In a typical experiment, 690 mg of SBMOF-1 powder was activated in high vacuum at 563 K for 10 h. Then the material was packed into a quartz column (5.8 mm i.d. × 150 mm) with silane treated glass wool filling the void space. A helium flow (1 cm^3 min^{-1}) was used to purge the adsorbent. The flow of He was then turned off while a gas mixture of $CH_4/C_2H_2/C_2H_4/C_2H_6$ (25:25:25:25, v/v) at 1 cm^3 min^{-1} was allowed to flow into the column. The effluent from the column was monitored using an online mass spectrometer (MS).[49]

2.4. Single Crystal XRD with Adsorbed Hydrocarbon Gases. For the gas loading, activated crystals of SBMOF-1 and SBMOF-2 were placed in a three-neck flask with ethane, ethylene, or acetylene flowing into the flask, and kept for 2 h. Further, the crystals were coated with Paratone oil, while keeping the gas flowing to maintain 1 bar conditions. Crystals of the C_2H_n-loaded SBMOF-1 and SBMOF-2 suitable for the single crystal X-ray diffraction were selected from the bulk using a polarizing microscope to determine crystal quality. Reflections for the compounds SBMOF-1:C_2H_2, SBMOF-1:C_2H_4, SBMOF-2:C_2H_2, and SBMOF-2:C_2H_4 were collected with 1° ω-scans at 100 K using a four-circle kappa Oxford Gemini diffractometer (λ= 0.710 73/1.541 84 Å). Raw intensity data were collected, integrated, and corrected for absorption effects using CrysAlisPRO software.[50] Reflections for SBMOF-1:C_2H_6 and SBMOF-2:C_2H_6 were collected at 100 K using a three-circle Bruker D8 diffractometer, equipped with an APEX II detector, with the X-ray wavelength λ = 0.413 28 Å, using 0.5° φ scans at the APS ChemMatCars (sector 15) beamline. Raw intensity data were collected, integrated, and corrected for absorption effects with the Apex II software suite.[51]

Structures of gas-loaded SBMOF-1 and SBMOF-2 were solved with direct methods using SHELXS-97 and refined with full-matrix least-squares on F^2 with SHELXTL-97 (Tables S2–S3).[52,53] During structure solution, atoms from the MOF framework were located first and refined with anisotropic displacement parameters. Hydrogen atoms were added to aromatic rings using geometrical constraints (HFIX command). After obtaining a satisfactory model of the framework, Fourier difference maps were calculated to locate the adsorbed gas molecules using the WinGX suite (Figure 4a).[54] All gas molecules were located from the strong electron density peaks and refined with anisotropic displacement parameters (Figure 4b,c). The occupancy of the C atoms from the adsorbed gases was also refined. The C–C distances in the hydrocarbon molecules were restrained to 1.20(1), 1.30(1), and 1.47(1) Å for acetylene, ethylene, and ethane, respectively. Hydrogen atoms on the hydrocarbon molecules were added with geometrical constrainst. In most cases the H atoms were visible on the electron density maps. Full details of the structure determinations have been deposited with the Cambridge Crystallographic Data Center under reference numbers 14205800–1420585 and are available free of charge from CCDC.

2.5. XRD–DSC. Differential enthalpy of adsorption of hydrocarbon gases (ΔH, kJ/mol_{MOF}) was measured with differential scanning calorimetry (DSC) at 298 K via vacuum-swing experimental procedure for C_1-C_2 in SBMOF-1 and C_1-nC_4 in SBMOF-2.

The collection of DSC data was accompanied by *in situ* powder diffraction measurments (XRD–DSC), allowing for the evaluation of the structural changes simultaneously with measuring gas adsorption enthalpy. We previously used the XRD–DSC method to study CO_2 adsorption in the presence of humidity in SBMOF-1 and other porous materials.[47,55,56] Isosteric heat of adsorption values (Q_{st}, kJ/mol_{GAS}) were obtained through the relation $Q_{st} = \Delta H/n_i$ (n_i = moles of the gas). Furthermore, Q_{st} values for C_1-nC_4 hydrocarbons were calculated for SBMOF-2 material with the virial method,[10] and the values of Q_{st} obtained with DSC and virial methods are in agreement (Table S4).

DOI: 10.1021/acs.chemmater.5b03792
Chem. Mater. 2016, 28, 1636–1646

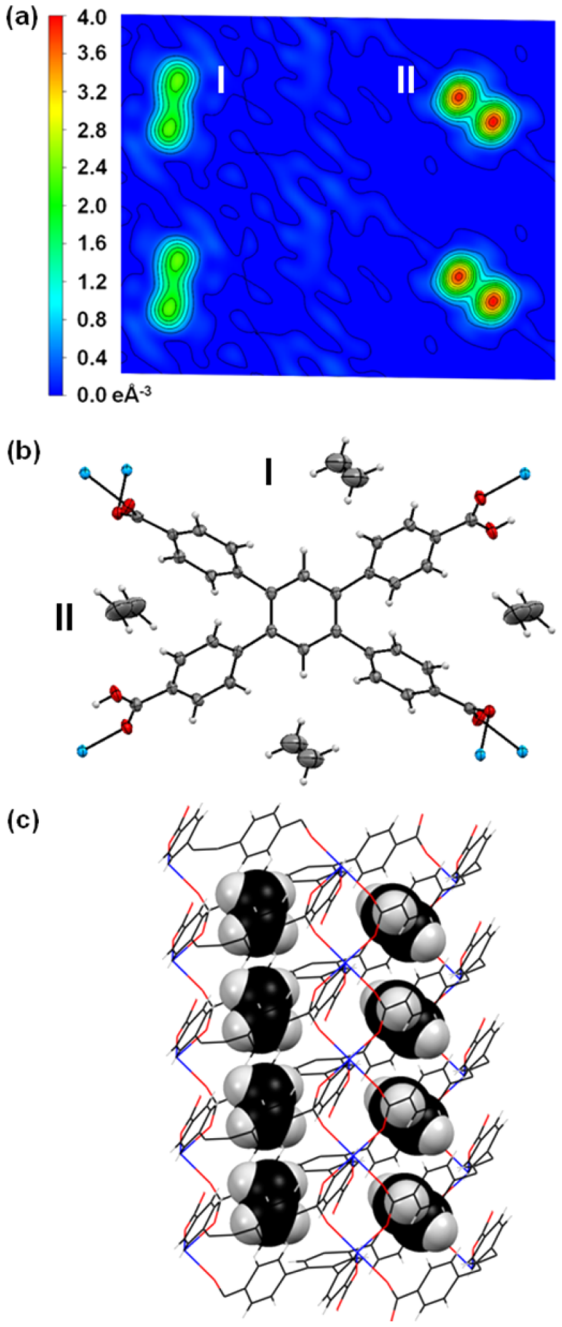

Figure 4. (a) Differential Fourier electron density map. Electron density on the left side indicates ethylene molecules adsorbed in channels of type I, and on the right side are channels of type II.[64] (b) Refined structure, atoms drawn at 50% probability level. (c) Structure of ethylene-loaded SBMOF-2, with gas molecules shown in space filling mode, and the network as wire frame. Blue spheres/wire represent Ca, red, O; black, C; gray, H.

Powder XRD−DSC measurements were collected with a Rigaku Ultima IV diffractometer (Cu Kα; λ = 1.5405 Å) with a D/teX Ultra high speed one-dimensional position sensitive detector. Powder X-ray pattern were collected within a range $5° \leq 2\theta \leq 37°$ (step size, 0.02°; counting time, 2s/step). The DSC measurements were performed using 9−10.5 mg of the sample in an aluminum crucible with an equal amount of Al_2O_3 in the reference crucible.

For the vacuum-swing experiments the sample was first heated to 563 K (SBMOF-1) or 523 K (SBMOF-2) under vacuum on the XRD−DSC stage, held at activation temperature for 5−10 h to ensure the activation, and then cooled to room temperature (RT). Further, the chamber was pressurized to 1 bar of hydrocarbon gas over the course of 15 s. After 120 (SBMOF-1) or 10 (SBMOF-2) minutes, when the DSC signal returned to the baseline, the chamber was evacuated to vacuum over the course of 15 s. In the case of SBMOF-1 strong interaction between the adsorbate and the framework leads to an incomplete removal under experimental vacuum conditions; as a result the enthalpy values were calculated on the basis of the averages of the exotherm of three different samples. In the case of SBMOF-2, all gases can be removed with vacuum, and a total of 6−8 cycles were completed. During the first cycle XRD data were collected.

3. RESULTS AND DISCUSSION

SBMOF-1 shows moderate adsorption of C_2H_n gases at 298 K; uptakes of 30.44, 30.0, and 29.5 cm^3/g were measured for acetylene, ethylene, and ethane, respectively. Methane is adsorbed at a lower amount than C_2H_n with uptake of 18.85 cm^3/g at 1 bar, 298 K (Figure 2a). The main difference between the adsorption of methane and C_2H_n is apparent when looking at the low pressure region of the isotherm. SBMOF-1 is saturated with C_2H_n at a very low pressure; for example, the ethane uptake of 27.3 cm^3/g at 0.1 bar is equal to over 90% of the total uptake at 1 bar. For comparison, methane adsorption at 0.1 bar (0.91 cm^3/g) is equivalent to less than 5% of the total uptake at 1 bar, and is more than 30 times lower than the ethane uptake at this pressure. Q_{st} of C_1−C_2 hydrocarbons in SBMOF-1 is relatively high,[5,29] with moderate differences between methane and C_2H_n (Table 1). The difference in adsorption behavior and heats of adsorption between methane and C_2H_n could be explained by higher electrostatic and dispersion interactions with the pore surface, and thus there is higher affinity of SBMOF-1 toward C_2 gases compared to small methane.[5] The gas adsorption selectivity calculated with the IAST method shows the C_2H_6/CH_4 selectivity of 74, C_2H_4/CH_4 of 73, and C_2H_2/CH_4 of 33 (Figure 2c). The C_2H_4/CH_4 and C_2H_2/CH_4 selectivities for SBMOF-1 are lower than those of the Fe-MOF-74 (700 and 200, respectively),[29] because of the presence of open metal sites in the activated framework in the latter case, while SBMOF-1 possesses no open metal sites. However, the 74 C_2H_6/CH_4 selectivity is more than 3 times higher than that for Fe-MOF-74 (20).[29]

SBMOF-2 uptake of C_2H_n is more than 2 times higher than that in the case of SBMOF-1 at 298 K and 1 bar, and the difference in maximum uptake between methane and C_2H_n is

Table 1. Hydrocarbon Adsorption in SBMOF-1 and SBMOF-2, Gas Uptake Measured with Gas Isotherms, and ΔH and Q_{st} Obtained through DSC Vacuum-Swing Experiments[45,52]

	SBMOF-1			SBMOF-2		
	uptake (wt %)	ΔH (kJ/mol$_{MOF}$)	Q_{st} (kJ/mol$_{GAS}$)	uptake (wt %)	ΔH (kJ/mol$_{MOF}$)	Q_{st} (kJ/mol$_{GAS}$)
CH_4	1.66	10(1)	28(3)	1.99	8.3(1)	18.0(2)
C_2H_2	3.53	16.3(1)	34.8(3)	7.51	55.4(4)	30.3(2)
C_2H_4	3.75	16.5(3)	35.0(5)	7.47	46.5(1)	29.2(1)
C_2H_6	3.96	15.6(3)	36.3(7)	8.33	53.5(1)	32.3(1)

DOI: 10.1021/acs.chemmater.5b03792
Chem. Mater. 2016, 28, 1636−1646

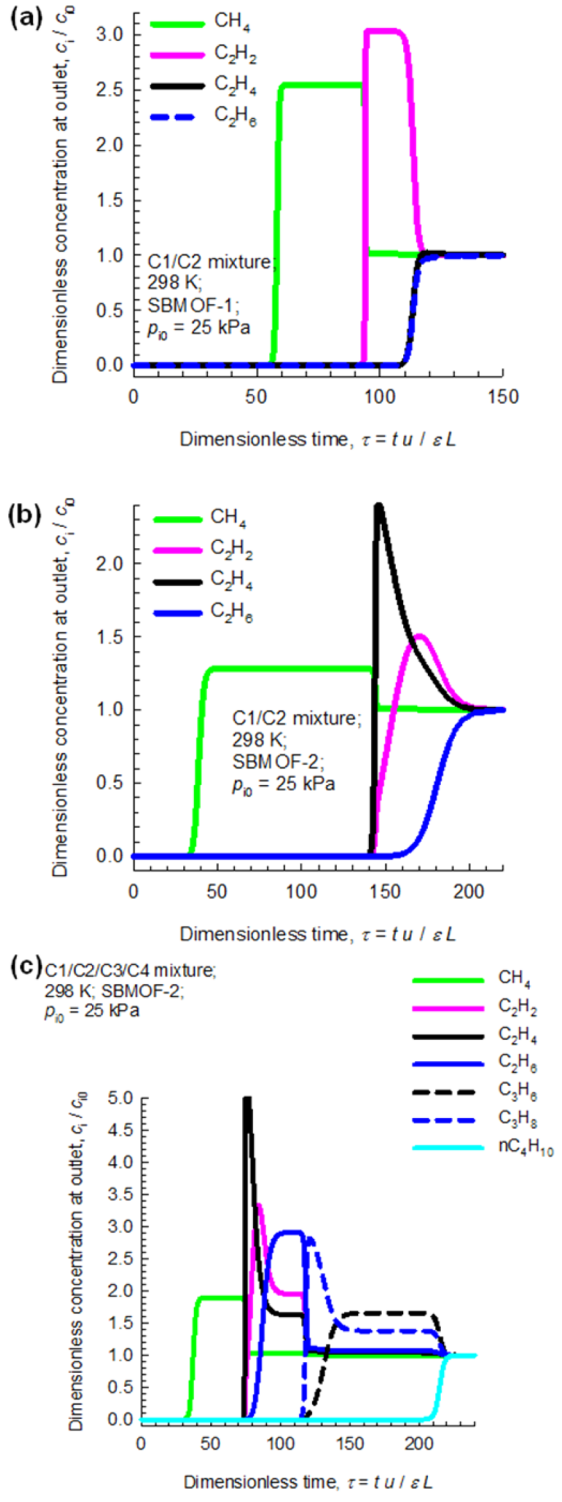

Figure 5. Transient breakthrough simulations for (a) separation of equimolar 4-component $CH_4/C_2H_2/C_2H_4/C_2H_6$ mixture using SBMOF-1 at 298 K, with partial pressures of 25 kPa each; (b) separation of an equimolar 4-component $CH_4/C_2H_2/C_2H_4/C_2H_6$ mixture using SBMOF-2 at 298 K, with partial pressures of 25 kPa each; (c) separation of an equimolar 7-component $CH_4/C_2H_2/C_2H_4/C_2H_6/C_3H_6/C_3H_8/C_4H_{10}$ mixture using SBMOF-2 at 298 K, with partial pressures of 25 kPa each.

more prominent than that for SBMOF-1. SBMOF-2 adsorbs 17.3 cm^3/g of methane at 298 K and 64.7, 59.8, and 62.2 cm^3/g of acetylene, ethylene, and ethane, respectively (Figure 2b).

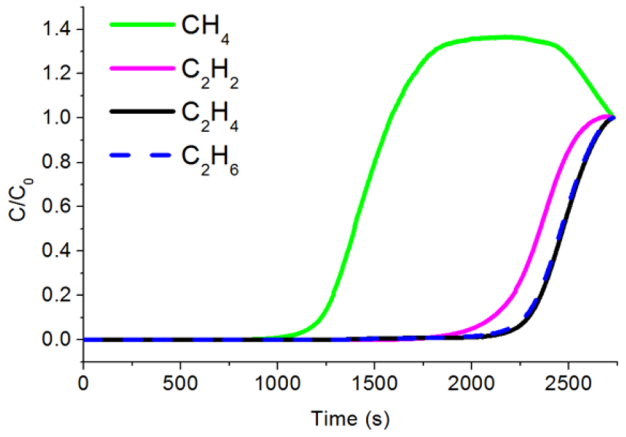

Figure 6. Experimental column breakthrough curve for a gas mixture of $CH_4/C_2H_2/C_2H_4/C_2H_6$ (25:25:25:25, v/v, 296 K, 1 bar) in a fixed bed packed with SBMOF-1.

The maximum uptake of C_2H_n in SBMOF-2 at 1 bar, 298 K, is lower than that for prototypical MOFs such as Fe-MOF-74 or MOF-5 but considerably higher than those of other porous materials extensively studied for hydrocarbon adsorption like ZIF-8 or RPM-3-Zn.[4,24,25,57] Q_{st} values for C_1-C_2 hydrocarbons adsorbed on SBMOF-2 are lower than in the case of the SBMOF-1 material (Table 1). The calculated C_2/C_1 selectivity in SBMOF-2 are 26 for C_2H_6/CH_4, 16 for C_2H_4/CH_4, and 18 for C_2H_2/CH_4 (Figure 2d), also lower than those calculated for SBMOF-1 and Fe-MOF-74.[29]

As in SBMOF-1, the only presumed interaction between gas molecules and the pore space is C−H···π; it is expected that the Q_{st} values will decrease with the C−C bond saturation.[58,59] However, the Q_{st} values of all three gases are quite similar to each other with the values of 34.8(3), 35.0(5), and 36.3(7) kJ/mol_{GAS} for acetylene, ethyelene, and ethane, respectively, suggesting that there is no significant influence of the C−C double or triple bond on the adsorbent−adsorbate interaction. In SBMOF-2 Q_{st} of all C_2H_n displays also similar values, with 30.3(2), 29.2(1), and 32.3(1) kJ/mol_{GAS} for ethane, ethylene, and acetylene, respectively. In both materials, however, we can see that ethane interacts with the pore surface with the highest energy of the three, in spite of the full saturation of the C−C bond, normally leading to the lower adsorbent−adsorbate energy.[58] The C_2H_n Q_{st} values for adsorption both on SBMOF-1 and SBMOF-2 suggest that the size of the molecule and the number of the H-pore surface interactions play a more important role on the resultant energy of adsorption than the saturation of the C−C bond.

SBMOF-2 was further tested for the adsorption of heavier C_3-nC_4 hydrocarbon gases. When looking on the gas adsorption of C_1-nC_4 alkanes on SBMOF-2, depicted in Figure 3a, we note that the adsorption follows the general trends observed for porous MOFs such as MOF-5.[27,60] SBMOF-2 saturates with longer alkanes at lower pressures, and the heavier gas generally displays a lower capacity than the lighter counterpart. Q_{st} becomes higher with an increase in the chain length due to the enhanced electrostatic and dispersion interactions between the adsorbed gases and the pore surfaces (Figure 3b).[61] In mixtures, longer chains are preferred over the smaller ones until the point of maximum selectivity, when the entropic cost of the long chain ordering affects the energy gained from the adsorption.[5]

The separation performance of industrial fixed bed adsorbents is dictated by a combination of adsorption selectivity and

DOI: 10.1021/acs.chemmater.5b03792
Chem. Mater. 2016, 28, 1636−1646

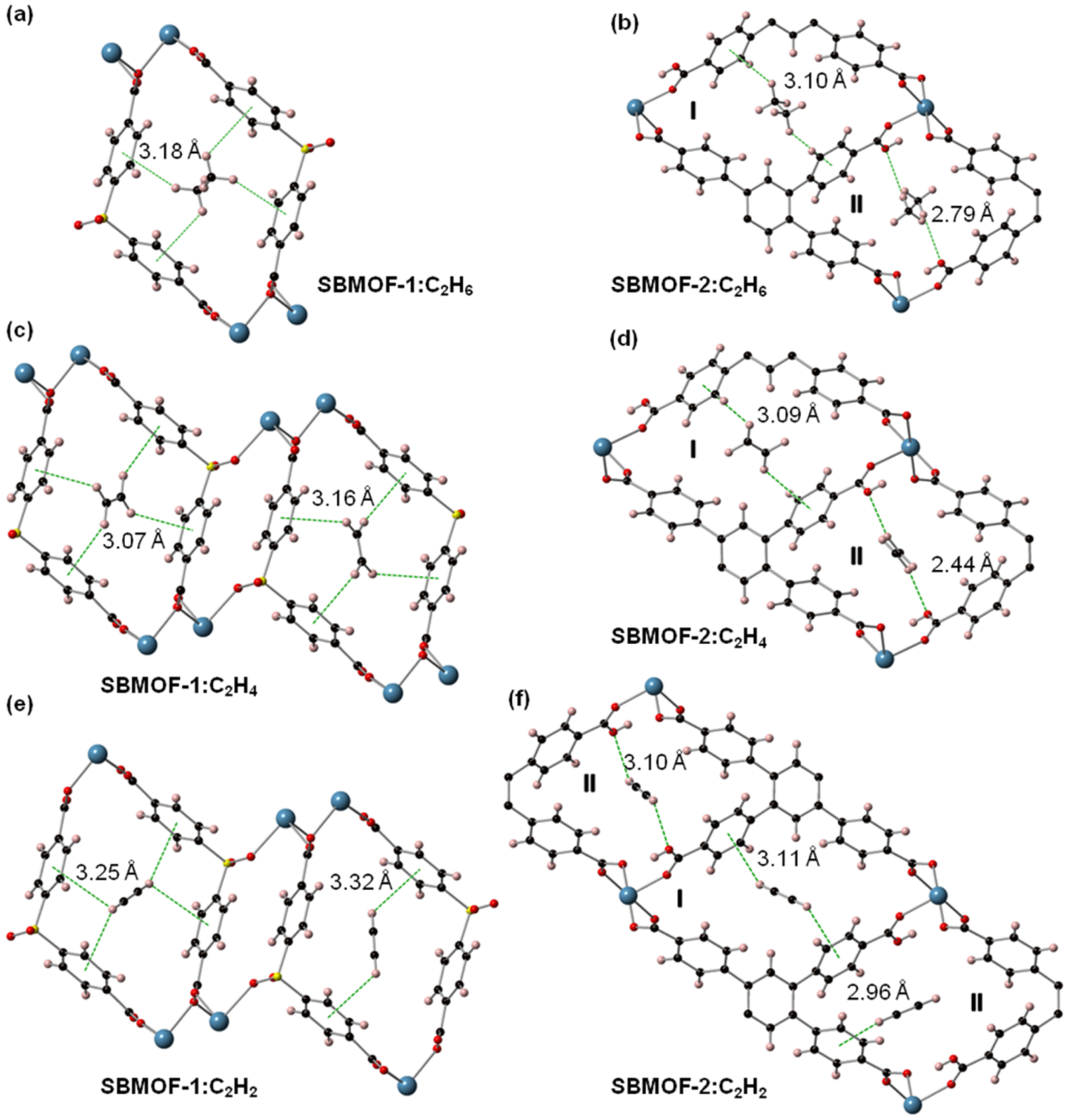

Figure 7. C_2 hydrocarbon adsorption sites in SBMOF-1 and SBMOF-2; shortest gas−sorption site distances are shown. In cases where gas displays disorder, the second orientation is shown in a consecutive pore: ethane adsorption sites in (a) SBMOF-1 and (b) SBMOF-2; ethylene adsorption sites in (c) SBMOF-1 and (d) SBMOF-2; acetylene adsorption sites in (e) SBMOF-1 and (f) SBMOF-2.

uptake capacity. In order to demonstrate the potential of SBMOF-1 and SBMOF-2 for separation of hydrocarbon mixtures, we performed transient breakthrough simulations. The results of the separation of an equimolar 4-component $CH_4/C_2H_2/C_2H_4/C_2H_6$ mixture using SBMOF-1 at 298 K, with partial pressures of 25 kPa each, are presented in Figure 5a. Since the C_2H_6/CH_4 and C_2H_4/CH_4 selectivities are practically the same (Figure 2b), the breakthroughs of C_2H_4, and C_2H_6 occur at practically the same time. The sequence of breakthroughs in Figure 5a indicates that SBMOF-1 has the potential for separating methane from C_2 hydrocarbon mixtures. Figure 5b depicts the corresponding transient breakthrough simulations for separation of C_1/C_2 mixtures using SBMOF-2. SBMOF-2 has significantly higher uptake capacities for hydrocarbons as compared to those of SBMOF-1 (Figure 2a,b); consequently, the breakthrough times with SBMOF-2 are significantly higher than the corresponding breakthrough times with SBMOF-1. Longer breakthrough times are desirable because this implies longer cycle times before the bed has to be regenerated. We therefore conclude that SBMOF-2 has superior separation performance for C_1/C_2 separations as compared to SBMOF-1. Finally, we studied how SBMOF-2 performs in separating C_1-nC_4 7-components mixtures. He et al. previously demonstrated the capability of M-MOF-74 for adsorptive "fractionation" of a $C_1/C_2/C_3$ hydrocarbon mixture.[62] We now established a similar fractionation capability of SBMOF-2. The breakthrough simulation data in Figure 5c demonstrate that SBMOF-2 has the ability to separate a 7-component

DOI: 10.1021/acs.chemmater.5b03792
Chem. Mater. 2016, 28, 1636−1646

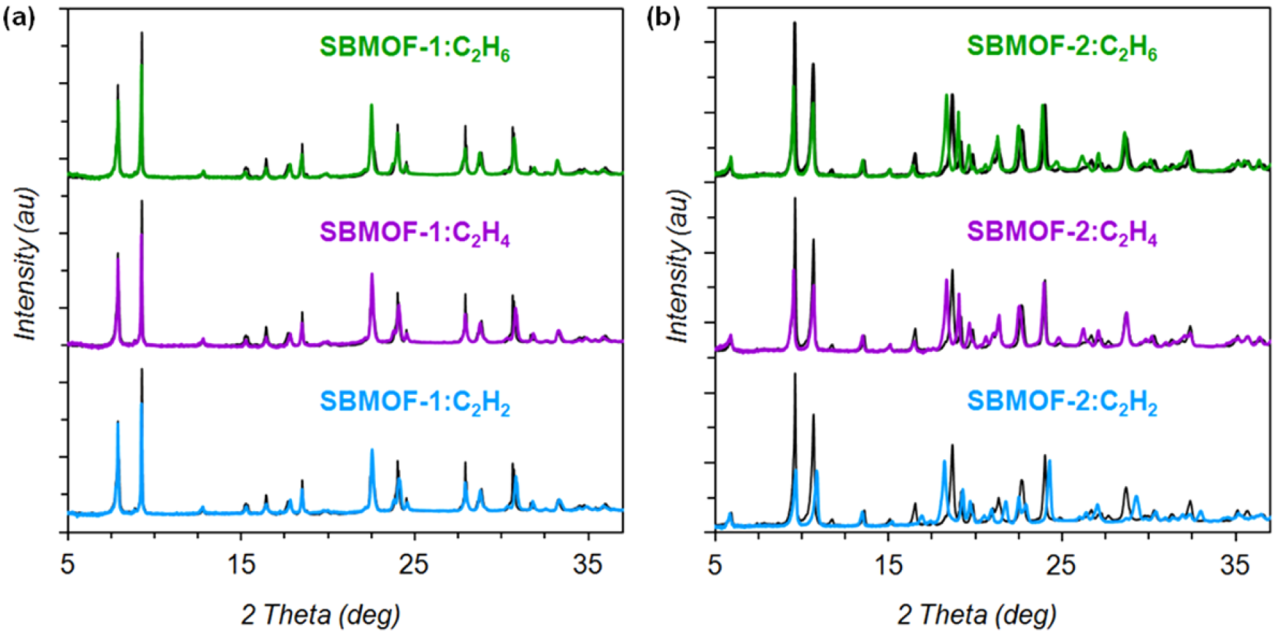

Figure 8. *In situ* PXRD collected at 1 atm pressure of C_2 hydrocarbons for (a) SBMOF-1 and (b) SBMOF-2. Black patterns represent activated samples.

$CH_4/C_2H_2/C_2H_4/C_2H_6/C_3H_6/C_3H_8/C_4H_{10}$ mixture into four different fractions, with increasing carbon numbers. The separation potential of SBMOF-2 is best appreciated by viewing the video animation that shows the transient traversal of gas phase concentrations of each of the seven components along the length of the fixed bed adsorber.

To supplement the simulated breakthrough we carried out the experimental breakthrough of an equimolar 4-component $CH_4/C_2H_2/C_2H_4/C_2H_6$ mixture using SBMOF-1 at 296 K. As shown in Figure 6, the experimental results are in excellent agreement with the simulations, showing the same gas separation sequence.

Further, we used a single crystal diffraction technique to determine the positions of adsorbed molecules in C_2H_n:SBMOF-1 and SBMOF-2 gas adducts. Refined occupancies of the adsorbed gases are on the average within less than 10% from the values obtained with gas adsorption experiments, confirming the validity of the technique (Table S5). The main presumed adsorbate−host interactions in SBMOF-1 and SBMOF-2 are C−H···π and C−H···O, with the latter appearing only in the channels of type II in SBMOF-2. Such interactions play a significant role in molecular crystal packing, protein folding, and molecular recognition.[59,61,63]

Analysis of the structural data of SBMOF-1:C_2H_n collected at 100 K revealed that, upon the loading with C_2H_n, sdb linkers rotated back to a parallel configuration observed in the as-synthesized material. Adsorbates locate on the inversion center at the center of the pore. In each structure, half of the C_2H_n molecule is within the asymmetric unit, and the second half is generated by the symmetry operation. Distances between hydrogen atoms of the C_2H_n molecules and neighboring phenyl ring centroids are within 3.07(4)−3.36(4) Å (Figure 7). The distance between adsorbate molecules along the channel is equivalent to lattice parameter *b*, 5.556(1) Å. The parallel orientation of the linkers provides the optimal geometry for the hydrocarbon molecules, forming cages of four phenyl rings. The ethylene molecule is oriented so that each of the H atoms is pointing toward the closest phenyl ring with the average distance of 3.15(9) Å. Ethane and acetylene gases locate in a similar fashion, with the average C−H···π distances of 3.4(1) and 3.23(8) Å, respectively. Acetylene and ethylene molecules display a 2-fold disorder while ethane shows no spatial disorder.

In SBMOF-2 gas adsorption sites differ between channels of types I and II. In the type I channels, the only presumed interactions are between hydrogen atoms of adsorbates and π clouds of organic linkers. The adsorbates locate within less than 4 Å distance to two or four phenyl rings at a time. The shortest C−H···π lengths, measured as a distance between the H atom and the phenyl centroid, are 3.11(2), 3.09(2), and 3.10(2) Å for acetylene, ethylene, and ethane, respectively (Figure 7). All three adsorbates can be located unambiguously from the electron density maps and all three, except acetylene in channels of type II, show no spatial disorder. In type II channels, the pore surface is decorated with multiple oxygen atoms including the −OH groups within the 4 Å from the center of the pore, and provides strong adsorption sites for the adsorbates through the presumed C−H···O interaction (Figure 7). The shortest C−H¨O distances are 3.10(2), 2.44(2), and 2.79(2) Å for acetylene, ethylene, and ethane, respectively.

In situ PXRD diffraction patterns of SBMOF-1 and SBMOF-2 confirm the adsorption mechanisms determined from single crystal diffraction. Upon gas loading, low angle peaks decrease with respect to higher angle reflections, consistent with the gas molecules occupying the pore space (Figure 8). Further, SBMOF-2 shows an increasing lattice change with the size of adsorbates as evident from the shifting of peaks' positions in the PXRD patterns (Figure 8b and Figures S17−S26). The lattice dimension *a* increases, and the α angle decreases from 5.1011(3) Å and 83.132(5)° in the activated sample to 5.2195(2) Å and 82.533(1)° in the SBMOF-2:C_2H_6, as determined from single crystal data and consistent with PXRD observations (Figures S21−S25). The *a* parameter is equivalent to the distance between adsorbed gas molecules along the pore. *In situ* PXRD data collected at 298 K from C_3−C_4 gas-loaded SBMOF-2 show a further increasing change between activated and gas-loaded material with increasing length of the hydrocarbon chain, suggesting that the

DOI: 10.1021/acs.chemmater.5b03792
Chem. Mater. 2016, 28, 1636−1646

SBMOF-2 framework is flexible and can accommodate larger molecules (Figures S29–S32).

4. CONCLUSIONS

We characterized adsorption mechanisms of ethane, ethylene, and acetylene in two microporous Ca-based metal organic frameworks, SBMOF-1 and SBMOF-2. Both materials are selective toward C_2H_n hydrocarbons over methane with the maximum C_2/C_1 selectivity of 74 for C_2H_6/CH_4 in SBMOF-1. The breakthrough simulation data confirmed that both SBMOF-1 and SBMOF-2 can separate C_1/C_2 mixtures. SBMOF-2 also has the ability to separate a 7-component $CH_4/C_2H_2/C_2H_4/C_2H_6/C_3H_6/C_3H_8/C_4H_{10}$ mixture into four different fractions, with increasing carbon numbers. Crystal structure of the gas-loaded SBMOF-1 shows that the framework behaves like a trap toward the C_2 hydrocarbons. The pore geometry in SBMOF-1 is optimal for the small C_2H_n molecules, as each of the pore segments is built with four phenyl rings, providing strong adsorption sites through C−H···π interactions. SBMOF-2 contains two types of channels: in the first type, only phenyl rings are accessible as adsorption sites for hydrocarbon molecules, while the second type contains multiple O atoms in close proximity to the center of the pore. The adsorbate−adsorbent interaction in SBMOF-2 appears to be similar to that in the SBMOF-1 case, except in those channels where additional polarizing −OH groups and oxygen atoms serve as strong adsorption sites for C_2H_n, through the C−H···O interaction. Those single crystal data are confirmed by the experimental gas adsorption and the XRD−DSC studies. *In situ* XRD−DSC results further suggest that SBMOF-2 displays some network flexibility, which allows accommodation of all the C_1-nC_4 hydrocarbon gases inside the pore space.

■ ASSOCIATED CONTENT

Supporting Information

The Supporting Information is available free of charge on the ACS Publications website at DOI: 10.1021/acs.chemmater.5b03792.

Figures S1−S32 and Tables S1−S5 (PDF)

Animation of transient traversal of gas phase concentrations of each of the seven components along the length of the fixed bed adsorber (AVI)

Crystallographic data for adsorption of C_2H_2 with SBMOF-1 (CIF)

Crystallographic data for adsorption of C_2H_4 with SBMOF-1 (CIF)

Crystallographic data for adsorption of C_2H_6 with SBMOF-1 (CIF)

Crystallographic data for adsorption of C_2H_2 with SBMOF-2 (CIF)

Crystallographic data for adsorption of C_2H_4 with SBMOF-2 (CIF)

Crystallographic data for adsorption of C_2H_6 with SBMOF-2 (CIF)

■ AUTHOR INFORMATION

Corresponding Authors

*E-mail: anna.plonka@yu.edu.

*E-mail: r.krishna@contact.uva.nl.

*E-mail: jingli@rutgers.edu.

Present Addresses

[▽]Physics Department, Yeshiva University, New York Office: 342, Building 555, Brookhaven National Laboratory, Upton, New York 11973, United States.

[○]Fundamental & Computational Science Directorate, Pacific Northwest National Laboratory, Richland, Washington 99352, United States.

Author Contributions

The manuscript was written through contributions of all authors.

Notes

The authors declare no competing financial interest.

■ ACKNOWLEDGMENTS

Synthetic strategies for development of SBMOF-2, SCXRD and DSC−XRD characterization work, and analysis of synchrotron data at Stony Brook by A.M.P., X.C., J.B.P., and W.R.W were supported by National Science Foundation Grant DMR-1231586. Structures of SBMOF-1:C_2H_2, SBMOF-1:C_2H_4, SBMOF-2:C_2H_2, and SBMOF-2:C_2H_4 were determined using the Stony Brook University single crystal diffractometer, obtained through the support of the NSF (Grant CHE-0840483). Structures of SBMOF-1:C_2H_6 and SBMOF-2:C_2H_6 were determined in ChemMatCars (Sector 15), Advanced Photon Source (APS), principally supported by the National Science Foundation/Department of Energy (NSF/CHE-0822838). Use of APS was supported by the U.S. Department of Energy, Office of Science, Office of Basic Energy Sciences, under Contract DE-AC02-06CH11357. The RU team acknowledges partial support for the gas adsorption work and IAST calculations by the U.S. Department of Energy, Office of Science, Office of Basic Energy Sciences, through Grant DE-FG02-08ER46491. Y.H. thanks KAUST for the Competitive Research Funds under Awards URF/1/1672-01-01.

■ REFERENCES

(1) Cao, C.; Chung, T.-S.; Liu, Y.; Wang, R.; Pramoda, K. Chemical Cross-Linking Modification of 6FDA-2, 6-DAT Hollow Fiber Membranes for Natural Gas Separation. *J. Membr. Sci.* **2003**, *216*, 257−268.

(2) Duan, X.; Zhang, Q.; Cai, J.; Cui, Y.; Wu, C.; Yang, Y.; Qian, G. A New Microporous Metal-Organic Framework with Potential for Highly Selective Separation Methane from Acetylene, Ethylene and Ethane at Room Temperature. *Microporous Mesoporous Mater.* **2014**, *190*, 32−37.

(3) Magnowski, N.; Avila, A.; Lin, C.; Shi, M.; Kuznicki, S. Extraction of Ethane from Natural Gas by Adsorption on Modified ETS-10. *Chem. Eng. Sci.* **2011**, *66*, 1697−1701.

(4) Banerjee, D.; Liu, J.; Thallapally, P. K. Separation of C_2 Hydrocarbons by Porous Materials: Metal Organic Frameworks as Platform. *Comments Inorg. Chem.* **2015**, *35*, 18−38.

(5) Herm, Z. R.; Bloch, E. D.; Long, J. R. Hydrocarbon Separations in Metal-Organic Frameworks. *Chem. Mater.* **2014**, *26*, 323−338.

(6) Jarvelin, H.; Fair, J. R. Adsorptive Separation of Propylene-Propane Mixtures. *Ind. Eng. Chem. Res.* **1993**, *32*, 2201−2207.

(7) Matsufuji, T.; Nishiyama, N.; Matsukata, M.; Ueyama, K. Separation of Butane and Xylene Isomers with MFI-Type Zeolitic Membrane Synthesized by a Vapor-Phase Transport Method. *J. Membr. Sci.* **2000**, *178*, 25−34.

(8) Li, B.; Zhang, Y.; Krishna, R.; Yao, K.; Han, Y.; Wu, Z.; Ma, D.; Shi, Z.; Pham, T.; Space, B.; Liu, J.; Thallapally, P. K.; Liu, J.; Chrzanowski, M.; Ma, S. Introduction of π-Complexation into Porous Aromatic Framework for Highly Selective Adsorption of Ethylene over Ethane. *J. Am. Chem. Soc.* **2014**, *136*, 8654−8660.

DOI: 10.1021/acs.chemmater.5b03792
Chem. Mater. 2016, 28, 1636−1646

(9) Getman, R. B.; Bae, Y.-S.; Wilmer, C. E.; Snurr, R. Q. Review and Analysis of Molecular Simulations of Methane, Hydrogen, and Acetylene Storage in Metal-Organic Frameworks. *Chem. Rev.* **2012**, *112*, 703−723.
(10) Suh, M. P.; Park, H. J.; Prasad, T. K.; Lim, D.-W. Hydrogen Storage in Metal-Organic Frameworks. *Chem. Rev.* **2012**, *112*, 782−835.
(11) Sumida, K.; Rogow, D. L.; Mason, J. A.; McDonald, T. M.; Bloch, E. D.; Herm, Z. R.; Bae, T.-H.; Long, J. R. Carbon Dioxide Capture in Metal-Organic Frameworks. *Chem. Rev.* **2012**, *112*, 724−781.
(12) Wu, H.; Gong, Q.; Olson, D. H.; Li, J. Commensurate Adsorption of Hydrocarbons and Alcohols in Microporous Metal Organic Frameworks. *Chem. Rev.* **2012**, *112*, 836−868.
(13) Li, J.-R.; Sculley, J.; Zhou, H.-C. Metal-Organic Frameworks for Separations. *Chem. Rev.* **2012**, *112*, 869−932.
(14) Stock, N.; Biswas, S. Synthesis of Metal-Organic Frameworks (MOFs): Routes to Various MOF Topologies, Morphologies, and Composites. *Chem. Rev.* **2012**, *112*, 933−969.
(15) Cohen, S. M. Postsynthetic Methods for the Functionalization of Metal-Organic Frameworks. *Chem. Rev.* **2012**, *112*, 970−1000.
(16) Kreno, L. E.; Leong, L.; Farha, O. K.; Allendorf, M.; Van Duyne, R. P.; Hupp, J. T. Metal-Organic Framework Materials as Chemical Sensors. *Chem. Rev.* **2012**, *112*, 1105−1125.
(17) Qiu, S.; Xue, M.; Zhu, G. Metal-Organic Framework Membranes: from Synthesis to Separation Application. *Chem. Soc. Rev.* **2014**, *43*, 6116−6140.
(18) Canivet, J.; Fateeva, A.; Guo, Y.; Coasne, B.; Farrusseng, D. Water Adsorption in MOFs: Fundamentals and Applications. *Chem. Soc. Rev.* **2014**, *43*, 5594−5617.
(19) Zhang, T.; Lin, W. Metal-Organic Frameworks for Artificial Photosynthesis and Photocatalysis. *Chem. Soc. Rev.* **2014**, *43*, 5982−5993.
(20) Ramaswamy, P.; Wong, N. E.; Shimizu, G. K. H. MOFs as Proton Conductors - Challenges and Opportunities. *Chem. Soc. Rev.* **2014**, *43*, 5913−5932.
(21) He, Y.; Zhou, W.; Qian, G.; Chen, B. Methane Storage in Metal-Organic Frameworks. *Chem. Soc. Rev.* **2014**, *43*, 5657−5678.
(22) Van de Voorde, B.; Bueken, B.; Denayer, J.; De Vos, D. Adsorptive Separation on Metal-Organic Frameworks in the Liquid Phase. *Chem. Soc. Rev.* **2014**, *43*, 5766−5788.
(23) Hu, Z.; Deibert, B. J.; Li, J. Luminescent Metal-Organic Frameworks for Chemical Sensing and Explosive Detection. *Chem. Soc. Rev.* **2014**, *43*, 5815−5840.
(24) Nijem, N.; Wu, H.; Canepa, P.; Marti, A.; Balkus, K. J., Jr; Thonhauser, T.; Li, J.; Chabal, Y. J. Tuning the Gate Opening Pressure of Metal-Organic Frameworks (MOFs) for the Selective Separation of Hydrocarbons. *J. Am. Chem. Soc.* **2012**, *134*, 15201−15204.
(25) Gücüyener, C.; van den Bergh, J.; Gascon, J.; Kapteijn, F. Ethane/Ethene Separation Turned on Its Head: Selective Ethane Adsorption on the Metal-Organic Framework ZIF-7 through a Gate-Opening Mechanism. *J. Am. Chem. Soc.* **2010**, *132*, 17704−17706.
(26) Farrusseng, D.; Daniel, C.; Gaudillere, C.; Ravon, U.; Schuurman, Y.; Mirodatos, C.; Dubbeldam, D.; Frost, H.; Snurr, R. Q. Heats of Adsorption for Seven Gases in Three Metal-Organic Frameworks: Systematic Comparison of Experiment and Simulation. *Langmuir* **2009**, *25*, 7383−7388.
(27) Jiang, J.; Sandler, S. I. Monte Carlo Simulation for the Adsorption and Separation of Linear and Branched Alkanes in IRMOF-1. *Langmuir* **2006**, *22*, 5702−5707.
(28) Munch, A. S.; Mertens, F. O. R. L. HKUST-1 as an Open Metal Site Gas Chromatographic Stationary Phase-Capillary Preparation, Separation of Small Hydrocarbons and Electron Donating Compounds, Determination of Thermodynamic Data. *J. Mater. Chem.* **2012**, *22*, 10228−10234.
(29) Bloch, E. D.; Queen, W. L.; Krishna, R.; Zadrozny, J. M.; Brown, C. M.; Long, J. R. Hydrocarbon Separations in a Metal-Organic Framework with Open Iron(II) Coordination Sites. *Science* **2012**, *335*, 1606−1610.
(30) Matsuda, R.; Kitaura, R.; Kitagawa, S.; Kubota, Y.; Belosludov, R. V.; Kobayashi, T. C.; Sakamoto, H.; Chiba, T.; Masaki, T.; Kawazoe, Y. Highly Controlled Acetylene Accommodation in a Metal-Organic Microporous Material. *Nature* **2005**, *436*, 238−241.
(31) Alaerts, L.; Kirschhock, C. E. A.; Maes, M.; van der Veen, M. A.; Finsy, V.; Depla, A.; Martens, J. A.; Baron, G. V.; Jacobs, P. A.; Denayer, J. F. M.; De Vos, D. E. Selective Adsorption and Separation of Xylene Isomers and Ethylbenzene with the Microporous Vanadium(IV) Terephthalate MIL-47. *Angew. Chem., Int. Ed.* **2007**, *46*, 4293−4297.
(32) Carrington, E. J.; Vitorica-Yrezabal, I. J.; Brammer, L. Crystallographic Studies of Gas Sorption in Metal-Organic Frameworks. *Acta Crystallogr., Sect. B: Struct. Sci., Cryst. Eng. Mater.* **2014**, *70*, 404−422.
(33) Samsonenko, D. G.; Kim, H.; Sun, Y.; Kim, G.-H.; Lee, H.-S.; Kim, K. Microporous Magnesium and Manganese Formates for Acetylene Storage and Separation. *Chem. - Asian J.* **2007**, *2*, 484−488.
(34) Kim, H.; Samsonenko, D. G.; Das, S.; Kim, G.-H.; Lee, H.-S.; Dybtsev, D. N.; Berdonosova, E. A.; Kim, K. Methane Sorption and Structural Characterization of the Sorption Sites in $Zn_2(bdc)_2(dabco)$ by Single Crystal X-ray Crystallography. *Chem. - Asian J.* **2009**, *4*, 886−891.
(35) Miller, S. R.; Wright, P. A.; Devic, T.; Serre, C.; Ferey, G.; Llewellyn, P. L.; Denoyel, R.; Gaberova, L.; Filinchuk, Y. Single Crystal X-ray Diffraction Studies of Carbon Dioxide and Fuel-Related Gases Adsorbed on the Small Pore Scandium Terephthalate Metal Organic Framework, $Sc_2(O_2CC_6H_4CO_2)_3$. *Langmuir* **2009**, *25*, 3618−3626.
(36) Zhang, J.-P.; Chen, X.-M. Optimized Acetylene/Carbon Dioxide Sorption in a Dynamic Porous Crystal. *J. Am. Chem. Soc.* **2009**, *131*, 5516−5521.
(37) Noro, S.-i.; Mizutani, J.; Hijikata, R.; Matsuda, R.; Sato, H.; Kitagawa, S.; Sugimoto, K.; Inubushi, Y.; Kubo, K.; Nakamura, T. Porous Coordination Polymers with Ubiquitous and Biocompatible Metals and a Neutral Bridging Ligand. *Nat. Commun.* **2015**, *6*, 5851.
(38) Mallick, A.; Saha, S.; Pachfule, P.; Roy, S.; Banerjee, R. Selective CO_2 and H_2 adsorption in a Chiral Magnesium-based Metal Organic Framework (Mg-MOF) with Open Metal Sites. *J. Mater. Chem.* **2010**, *20*, 9073−80.
(39) Britt, D.; Furukawa, H.; Wang, B.; Glover, T. G.; Yaghi, O. M. Highly Efficient Separation of Carbon Dioxide by a Metal-Organic Framework Replete with Open Metal sites. *Proc. Natl. Acad. Sci. U. S. A.* **2009**, *106*, 20637−40.
(40) Banerjee, D.; Zhang, Z.; Plonka, A. M.; Li, J.; Parise, J. B. A Calcium Coordination Framework Having Permanent Porosity and High CO_2/N_2 Selectivity. *Cryst. Growth Des.* **2012**, *12*, 2162−2165.
(41) Plonka, A. M.; Banerjee, D.; Parise, J. B. Effect of Ligand Structural Isomerism in Formation of Calcium Coordination Networks. *Cryst. Growth Des.* **2012**, *12*, 2460−2467.
(42) Chen, X.; Plonka, A. M.; Banerjee, D.; Parise, J. B. Synthesis, Structures and Photoluminescence Properties of a Series of Alkaline Earth Metal-Based Coordination Networks Synthesized Using Thiophene-Based Linkers. *Cryst. Growth Des.* **2013**, *13*, 326−332.
(43) Chen, X.; Plonka, A. M.; Banerjee, D.; Krishna, R.; Schaef, H. T.; Ghose, S.; Thallapally, P. K.; Parise, J. B. Direct Observation of Xe and Kr Adsorption in a Xe-selective Microporous Metal Organic Framework. *J. Am. Chem. Soc.* **2015**, *137*, 7007−7010.
(44) Myers, A. L.; Prausnitz, J. M. Thermodynamics of Mixed-Gas Adsorption. *AIChE J.* **1965**, *11*, 121−127.
(45) Krishna, R. Methodologies for Evaluation of Metal-Organic Frameworks in Separation Applications. *RSC Adv.* **2015**, *5*, 52269−52295.
(46) Spek, A. Single-Crystal Structure Validation with the Program PLATON. *J. Appl. Crystallogr.* **2003**, *36*, 7−13.
(47) Plonka, A. M.; Banerjee, D.; Woerner, W. R.; Zhang, Z.; Nijem, N.; Chabal, Y. J.; Li, J.; Parise, J. B. Mechanism of Carbon Dioxide Adsorption in a Highly Selective Coordination Network Supported by Direct Structural Evidence. *Angew. Chem., Int. Ed.* **2013**, *52*, 1692−1695.

DOI: 10.1021/acs.chemmater.5b03792
Chem. Mater. 2016, 28, 1636−1646

(48) Cessford, N. F.; Seaton, N. A.; Düren, T. Evaluation of Ideal Adsorbed Solution Theory as a Tool for the Design of Metal-Organic Framework Materials. *Ind. Eng. Chem. Res.* **2012**, *51*, 4911−4921.
(49) Zhao, Y.; Liu, X.; Han, Y. Microporous Carbonaceous Adsorbents for CO_2 Separation via Selective Sdsorption. *RSC Adv.* **2015**, *5*, 30310−30.
(50) Oxford Diffraction. *CrysAlis Pro and CrysAlis RED*; Oxford Diffraction Ltd.: Abingdon, U.K., 2007.
(51) Bruker AXS Inc. *APEX II Software Package*; Bruker Analytical X-ray System Inc.: Madison, WI, 2005.
(52) Sheldrick, G. A Short History of SHELX. *Acta Crystallogr., Sect. A: Found. Crystallogr.* **2008**, *64*, 112−122.
(53) Sheldrick, G. *SHELXTL, Structure Determination Software Programs*; Bruker Analytical X-ray System Inc.: Madison, WI, 1997.
(54) Farrugia, L. WinGX and ORTEP for Windows: an Update. *J. Appl. Crystallogr.* **2012**, *45*, 849−854.
(55) Plonka, A. M.; Banerjee, D.; Woerner, W. R.; Zhang, Z.; Li, J.; Parise, J. B. Effect of Ligand Geometry on Selective Gas-Adsorption: the Case of a Microporous Cadmium Metal Organic Framework with a V-shaped Linker. *Chem. Commun.* **2013**, *49*, 7055−7057.
(56) Woerner, W. R.; Plonka, A. M.; Chen, X.; Banerjee, D.; Thallapally, P. K.; Parise, J. B. Simultaneous in situ X-ray Diffraction and Calorimetric Studies as a Tool to Evaluate Gas Adsorption in Microporous Materials. *J. Phys. Chem. C* **2016**, *120*, 360.
(57) Fairen-Jimenez, D.; Galvelis, R.; Torrisi, A.; Gellan, A. D.; Wharmby, M. T.; Mellot-Draznieks, C.; Duren, T. Flexibility and Swing Effect on the Adsorption of Energy-Related Gases on ZIF-8: Combined Experimental and Simulation Study. *Dalton Trans.* **2012**, *41*, 10752−10762.
(58) Tsuzuki, S.; Fujii, A. Nature and Physical Origin of CH/π Interaction: Significant Difference from Conventional Hydrogen Bonds. *Phys. Chem. Chem. Phys.* **2008**, *10*, 2584−2594.
(59) Melandri, S. "Union is strength": How Weak Hydrogen Bonds Become Stronger. *Phys. Chem. Chem. Phys.* **2011**, *13*, 13901−13911.
(60) Düren, T.; Snurr, R. Q. Assessment of Isoreticular Metal-Organic Frameworks for Adsorption Separations: A Molecular Simulation Study of Methane/n-Butane Mixtures. *J. Phys. Chem. B* **2004**, *108*, 15703−15708.
(61) Nishio, M.; Umezawa, Y.; Honda, K.; Tsuboyama, S.; Suezawa, H. CH/π Hydrogen Bonds in Organic and Organometallic Chemistry. *CrystEngComm* **2009**, *11*, 1757−1788.
(62) He, Y.; Krishna, R.; Chen, B. Metal-Organic Frameworks with Potential for Energy-Efficient Adsorptive Separation of Light Hydrocarbons. *Energy Environ. Sci.* **2012**, *5*, 9107−9120.
(63) Tsuzuki, S.; Fujii, A. Nature and Physical Origin of CH/π Interaction: Significant Difference from Conventional Hydrogen Bonds. *Phys. Chem. Chem. Phys.* **2008**, *10*, 2584−2594.
(64) Momma, K.; Izumi, F. VESTA 3 for Three-Dimensional Visualization of Crystal, Volumetric and Morphology data. *J. Appl. Crystallogr.* **2011**, *44*, 1272−1276.

DOI: 10.1021/acs.chemmater.5b03792
Chem. Mater. 2016, 28, 1636−1646

Light Hydrocarbons Adsorption Mechanisms in Two Calcium-based Microporous Metal Organic Frameworks

Anna M. Plonka,[1,*,†] Xianyin Chen,[2] Hao Wang,[3] Rajamani Krishna,[4,*] Xinglong Dong,[5] Debasis Banerjee,[3,††] William R. Woerner,[1] Yu Han,[5] Jing Li[3,*] and John B. Parise[1,2,6]

[1]Department of Geosciences, Stony Brook University, Stony Brook, 11794 NY, USA

[2]Department of Chemistry, Stony Brook University, Stony Brook, 11794 NY, USA

[3]Department of Chemistry and Chemical Biology, Rutgers University, Piscataway, 08854 NJ, USA

[4]Van't Hoff Institute for Molecular Sciences, University of Amsterdam, Science Park 904, 1098 XH Amsterdam, The Netherlands

[5] King Abdullah University of Science and Technology, Thuwal 23955-6900, Kingdom of Saudi Arabia

[6]Photon Sciences, Brookhaven National Laboratory, Upton, NY 11973, USA

*Corresponding Authors: anna.plonka@yu.edu, jingli@rutgers.edu, r.krishna@contact.uva.nl

Supplementary materials contain supplementary text, supplementary Figures S1-S32 and supplementary Tables S1- S5.

Supplementary text

Ideal Adsorbed Solution Theory

An ideal adsorbed solution theory (IAST), developed by Myers and Prausnitz,[1] is used to simulate the competitive loading of a gas mixture on a material, based on adsorption isotherms of individual components.[2]

The relation between mole fraction of the adsorbed phase (x_i) and the mole fraction of the bulk gaseous phase (y_i) of the component *i* at a given pressure (p) is:

$$p \times y_i = p_i^0(\pi^*)x_i \qquad (1)$$

where p_i^0 is the pressure of component *i* and π^* is the spreading pressure of the gas mixture. π^* is described by:

$$\pi^* = \int_0^{p_i^0} \frac{q_i}{p} dp \qquad (2)$$

where *qi* is the adsorbed amount of component *i* under pressure *p* obtained via single component isotherm.

At equilibrium the spreading pressure of each component is the same:

$$\pi_i^* = \pi_j^* \ (i \neq j) \qquad (3)$$

The adsorption selectivity ($S_{i/j}$) of component *i* over *j* is defined as:

$$S_{i/j} = \frac{x_i / x_j}{y_i / y_j} \qquad (4)$$

To perform the IAST calculations, an adsorption model is needed in order to fit a discrete set of adsorption data from single-component isotherms with a continuous function.[2] In this work we used a Dual-site Langmuir-Freundlich (DSLF) model for the fitting of the adsorption isotherms. There is no limitation on the adsorption model used, but DSLF is found to fit the isotherms in the most precise manner.[3-6]

The DSLF model can be expressed as follows:

$$N = N_1^{max} \times \frac{b_1 p^{1/n_1}}{1 + b_1 p^{1/n_1}} + N_2^{max} \times \frac{b_2 p^{1/n_2}}{1 + b_2 p^{1/n_2}} \qquad (5)$$

Here, p is the pressure of the bulk gas at equilibrium with the adsorbed phase, N is the adsorbed amount per mass of the adsorbent, N_1^{max} and N_2^{max} are the saturation capacities of sites 1 and 2, respectively; b_1 and b_2 are the affinity coefficients of sites 1 and 2, and n_1 and n_2 represent the deviations from an ideal homogeneous surface.

The isosteric heats of adsorption can be determined by the Clausius-Clapeyron equation as the slop of ln(p) vs 1/T at loading n.

$$(\ln p)_n = (\frac{Q_{st}}{R})(\frac{1}{T}) + C$$

Supplementary figures

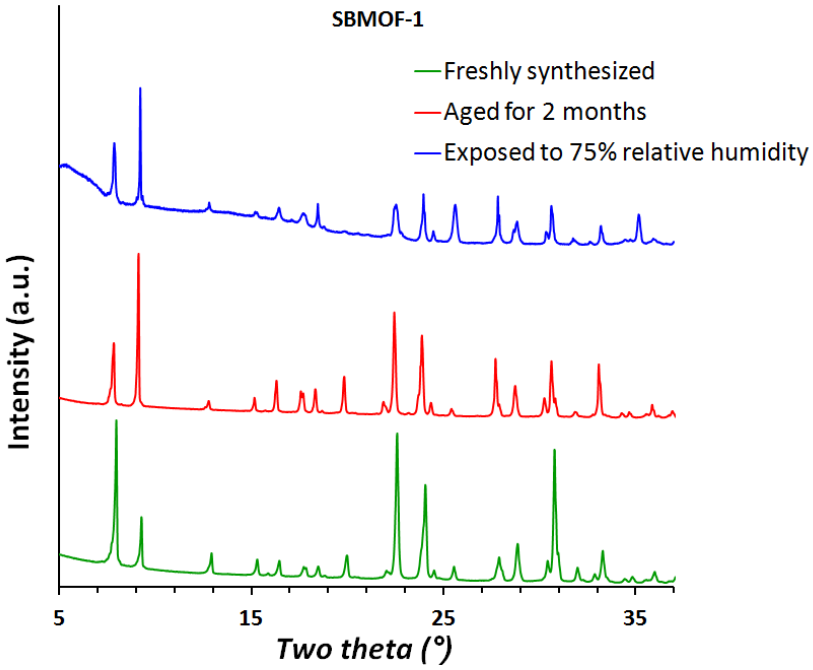

Figure S1. PXRD patterns of freshly synthesized, aged and humidity-exposed SBMOF-1.

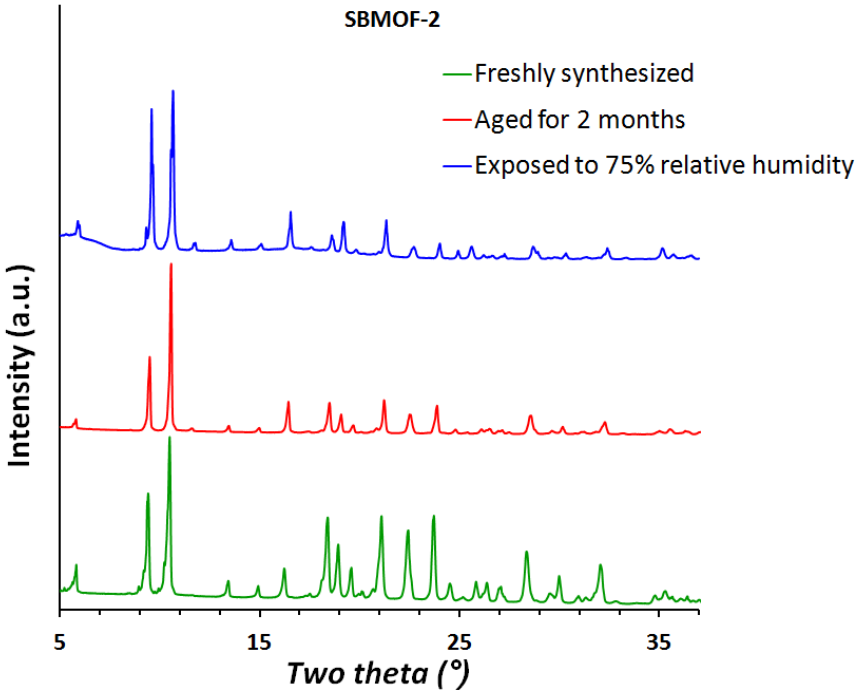

Figure S2. PXRD patterns of freshly synthesized, aged and humidity-exposed SBMOF-2.

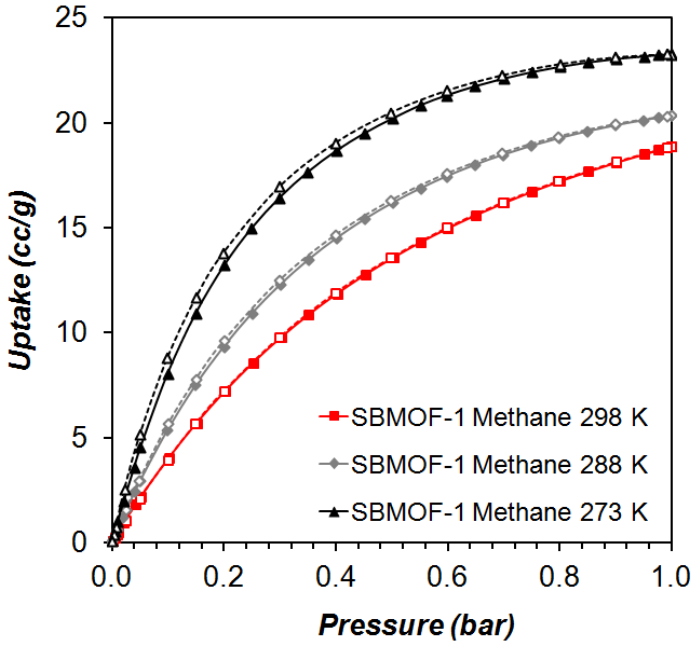

Figure S3. Methane adsorption on SBMOF-1, full symbols indicate adsorption points, open symbols – desorption.

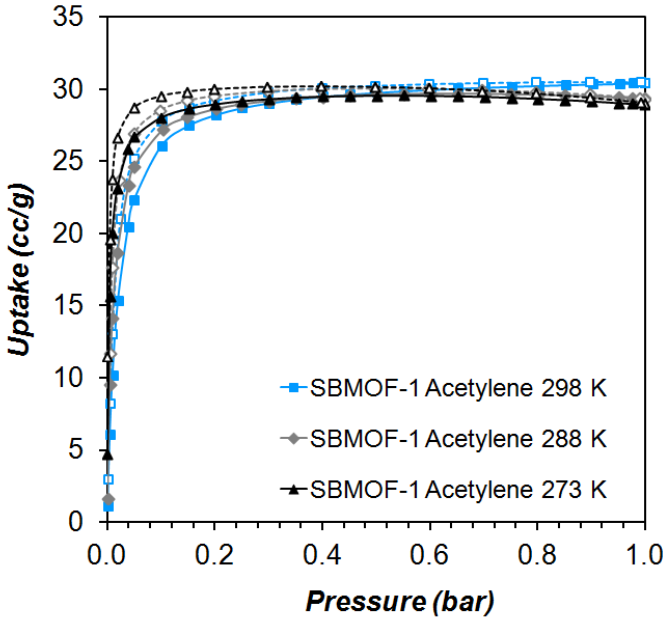

Figure S4. Acetylene adsorption on SBMOF-1, full symbols indicate adsorption points, open symbols – desorption.

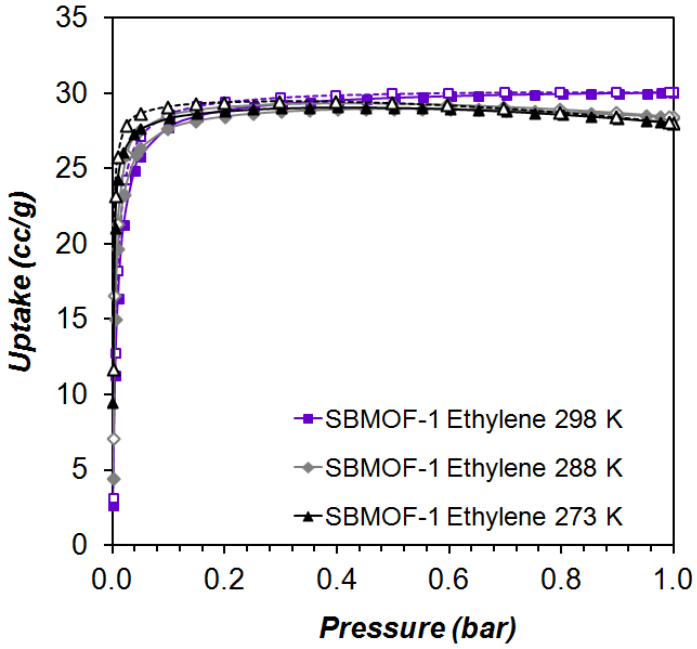

Figure S5. Ethylene adsorption on SBMOF-1, full symbols indicate adsorption points, open symbols – desorption.

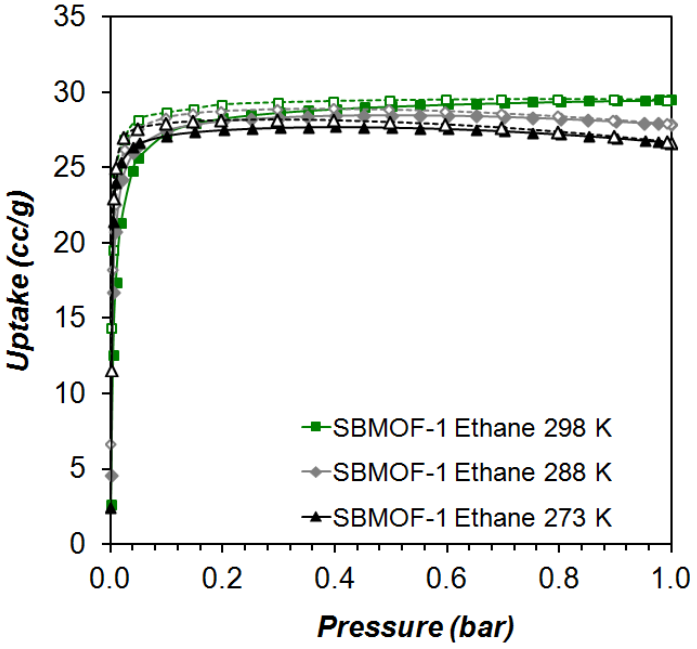

Figure S6. Ethane adsorption on SBMOF-1, full symbols indicate adsorption points, open symbols – desorption.

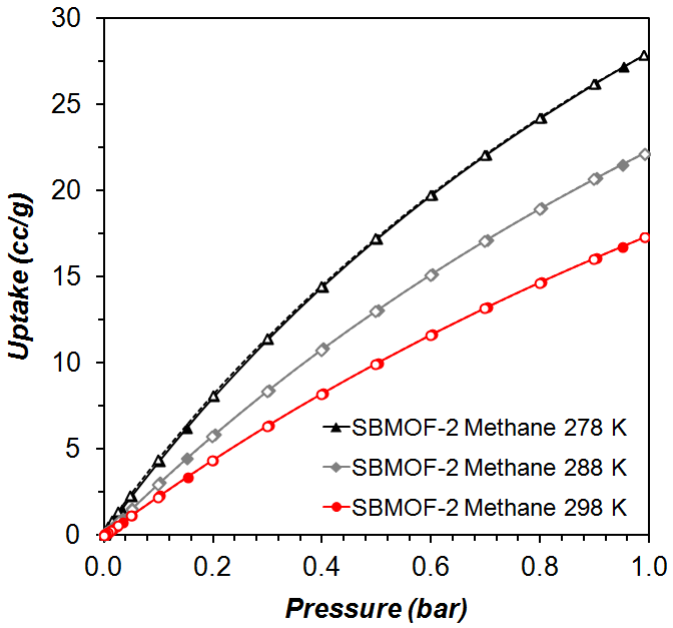

Figure S7. Methane adsorption on SBMOF-2, full symbols indicate adsorption points, open symbols – desorption.

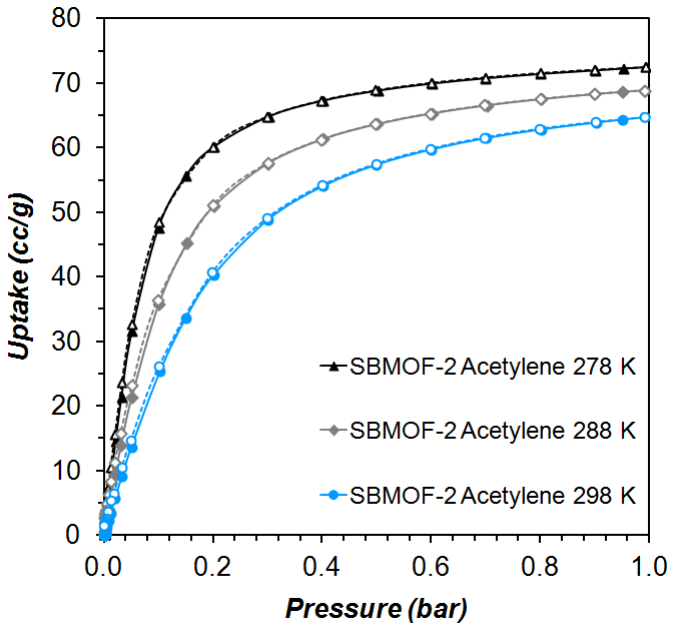

Figure S8. Acetylene adsorption on SBMOF-2, full symbols indicate adsorption points, open symbols – desorption.

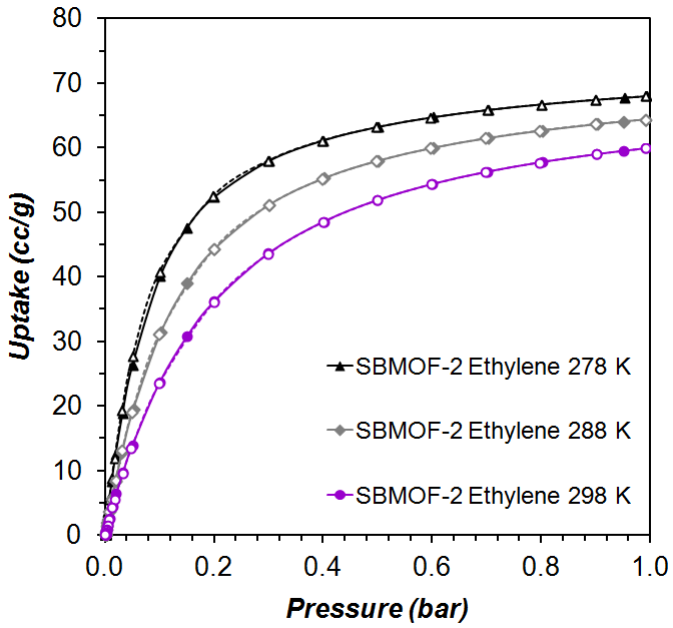

Figure S9. Ethylene adsorption on SBMOF-2, full symbols indicate adsorption points, open symbols – desorption.

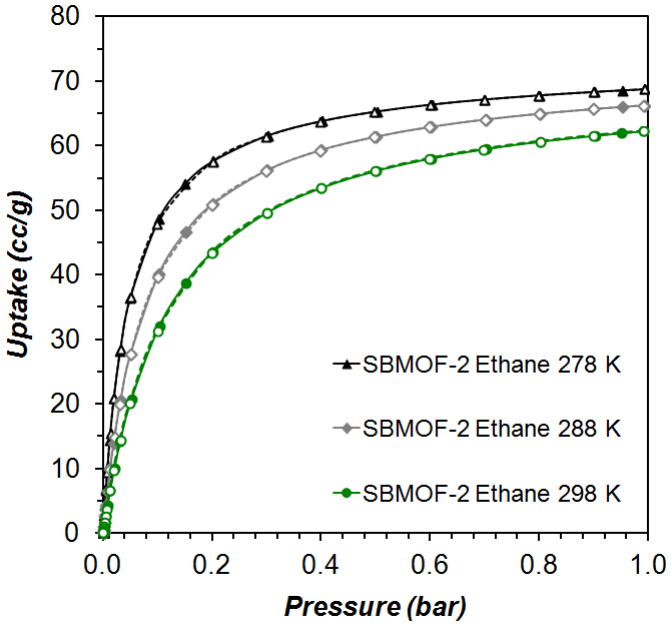

Figure S10. Ethane adsorption on SBMOF-2, full symbols indicate adsorption points, open symbols – desorption.

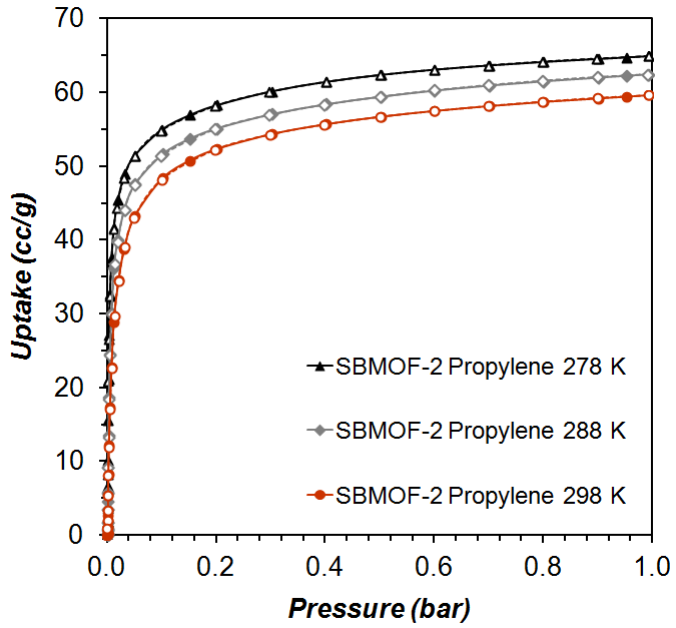

Figure S11. Propylene adsorption on SBMOF-2, full symbols indicate adsorption points, open symbols – desorption.

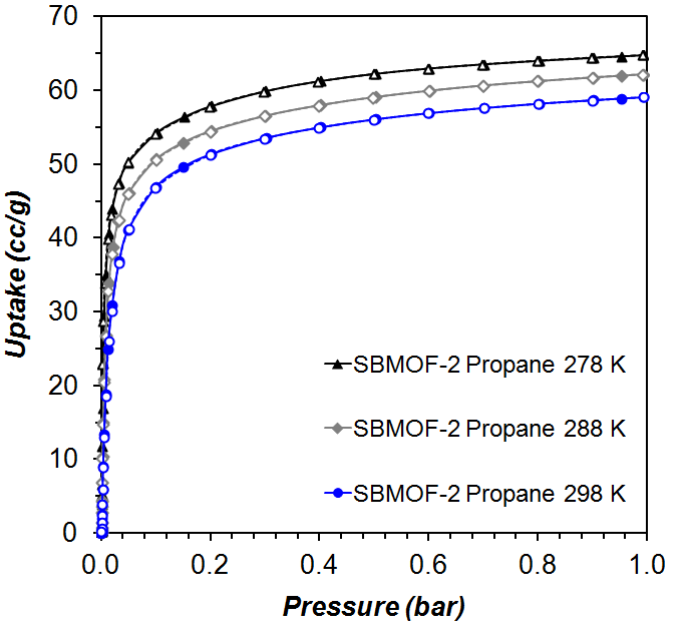

Figure S12. Propane adsorption on SBMOF-2, full symbols indicate adsorption points, open symbols – desorption.

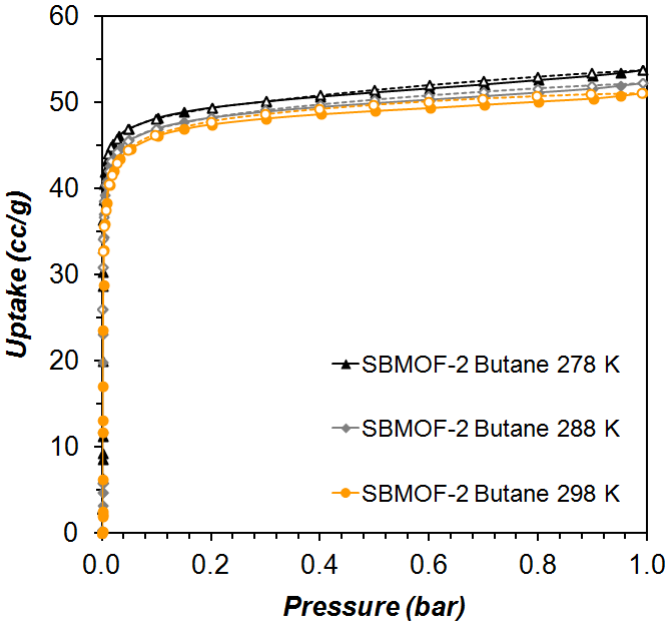

Figure S13. Butane adsorption on SBMOF-2, full symbols indicate adsorption points, open symbols – desorption.

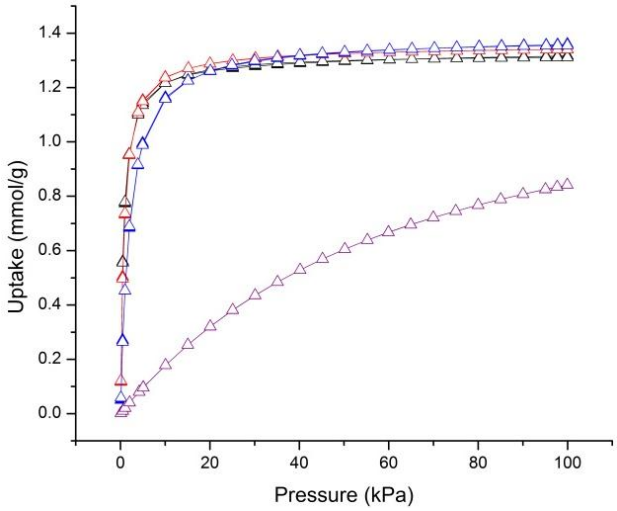

Figure S14. Comparison between experimental adsorption isotherms (298 K) and DSLF fits for C_2H_6 (black), C_2H_4 (red), C_2H_2 (blue), CH_4 (purple) on SBMOF-1. The solid and open symbols represent experimental isotherms and DSLF fits, respectively.

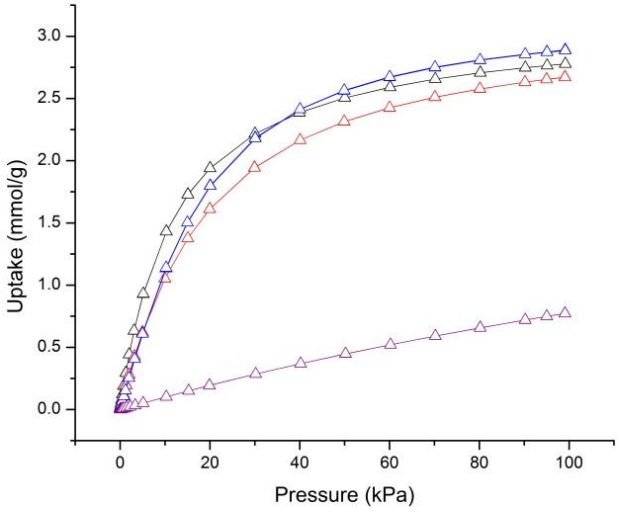

Figure S15. Comparison between experimental adsorption isotherms (298 K) and DSLF fits for C_2H_6 (black), C_2H_4 (red), C_2H_2 (blue), CH_4 (purple) on SBMOF-2. The solid and open symbols represent experimental isotherms and DSLF fits, respectively.

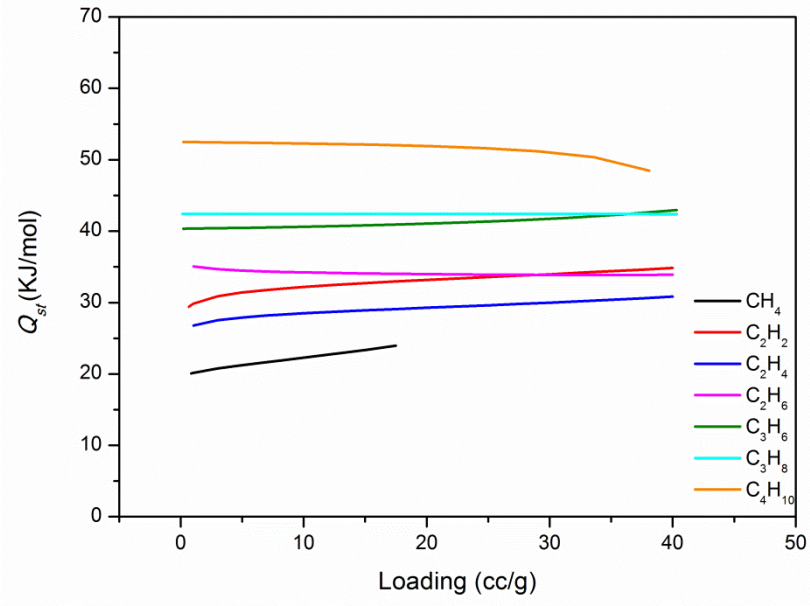

Figure S16. Isosteric heat of adsorption for C_1-nC_4 hydrocarbon gases on SBMOF-2 calculated with the DLSF method.

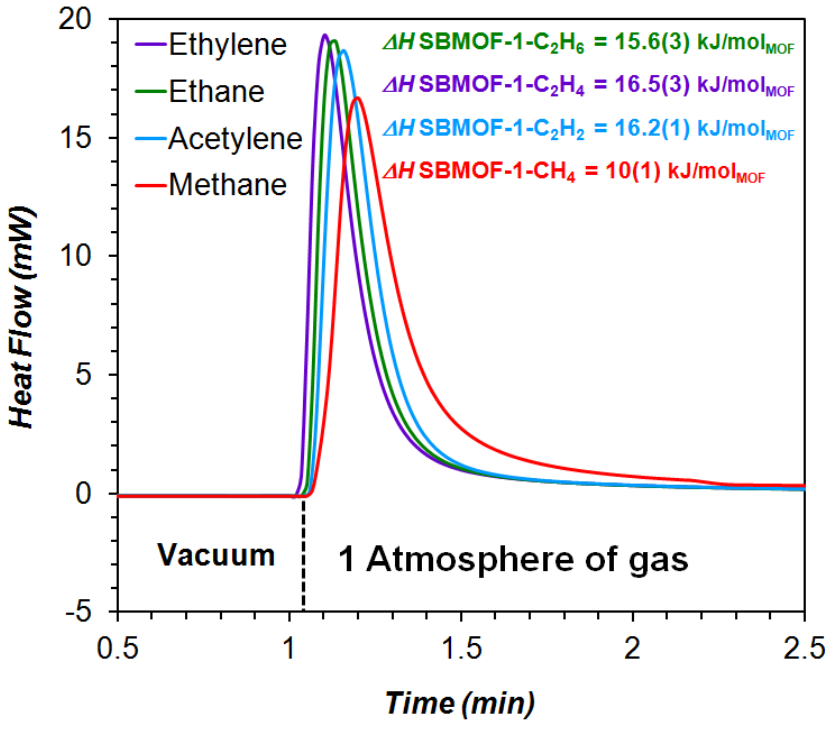

Figure S17. DSC signals measured upon loading activated SBMOF-1 with C_1-C_2 gases.

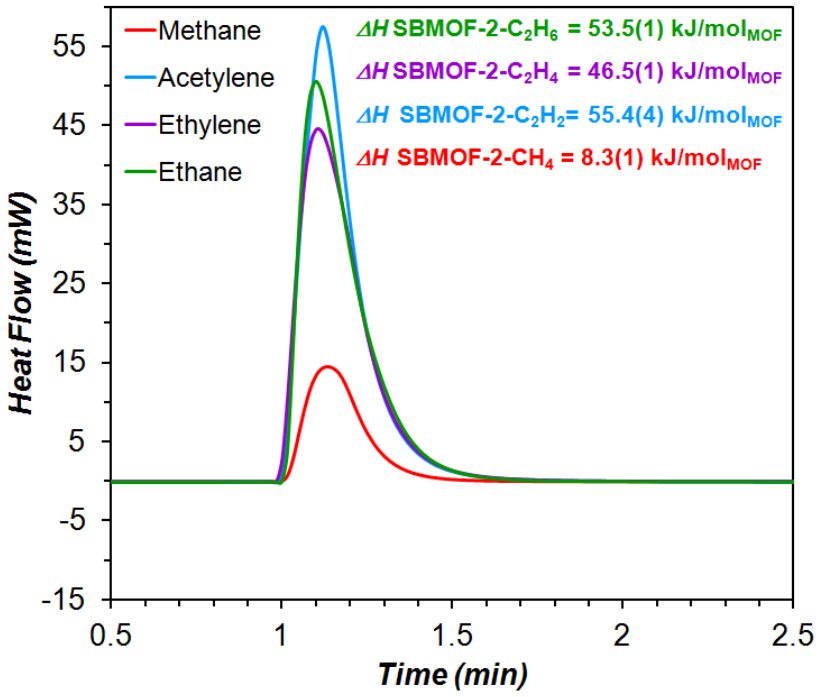

Figure S18. DSC signals measured upon loading activated SBMOF-2 with C_1-C_2 gases.

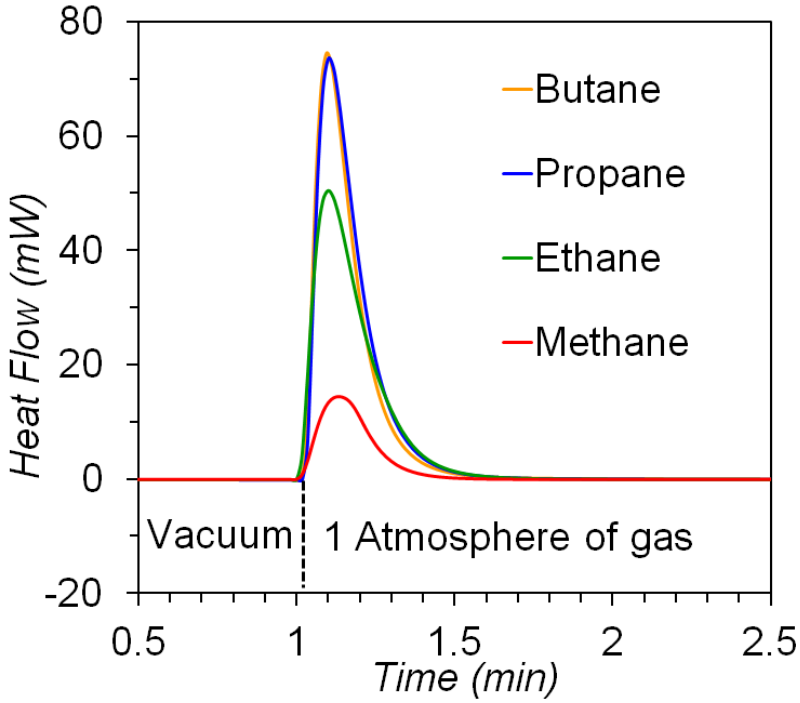

Figure S19. DSC signals measured upon loading activated SBMOF-2 with C_1-C_4 alkanes.

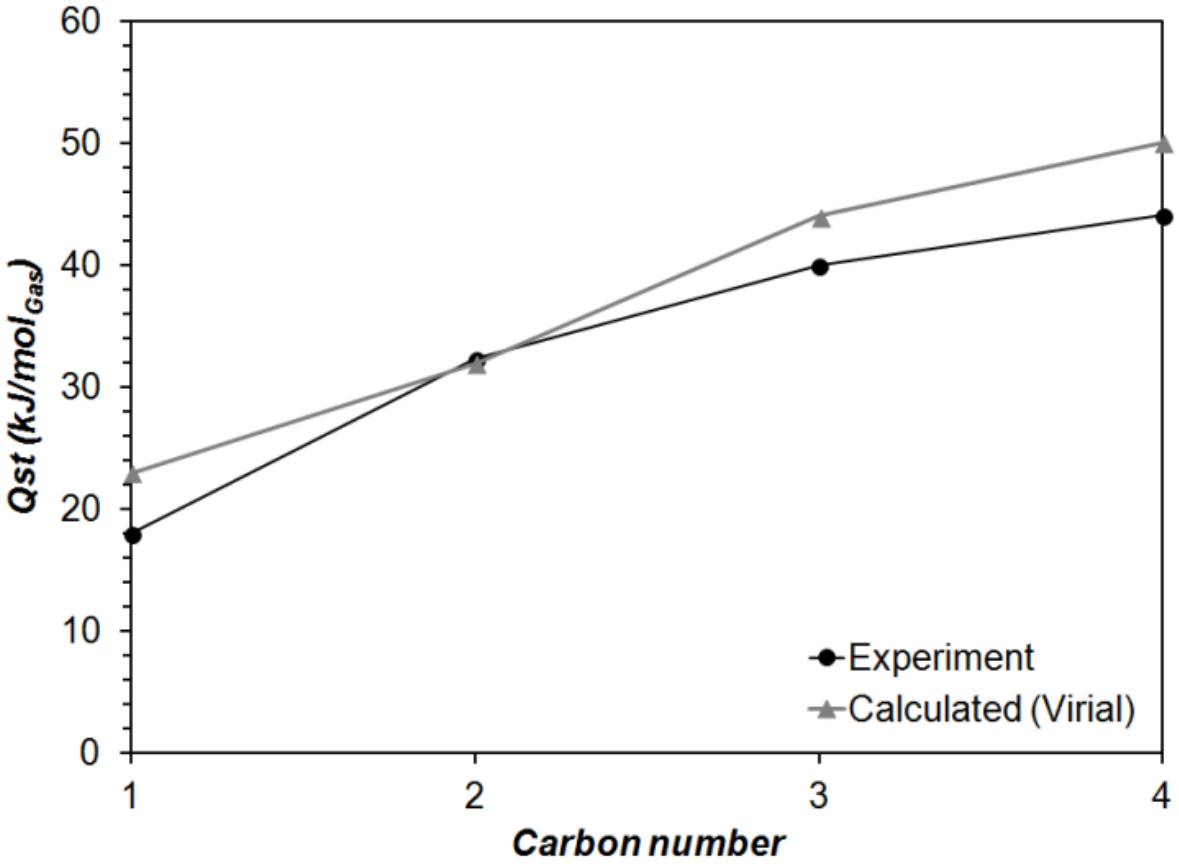

Figure S20. Trends in experimental and calculated Q_{st} of C_1-nC_4 alkanes adsorbed on SBMOF-2 as a function of carbon number.

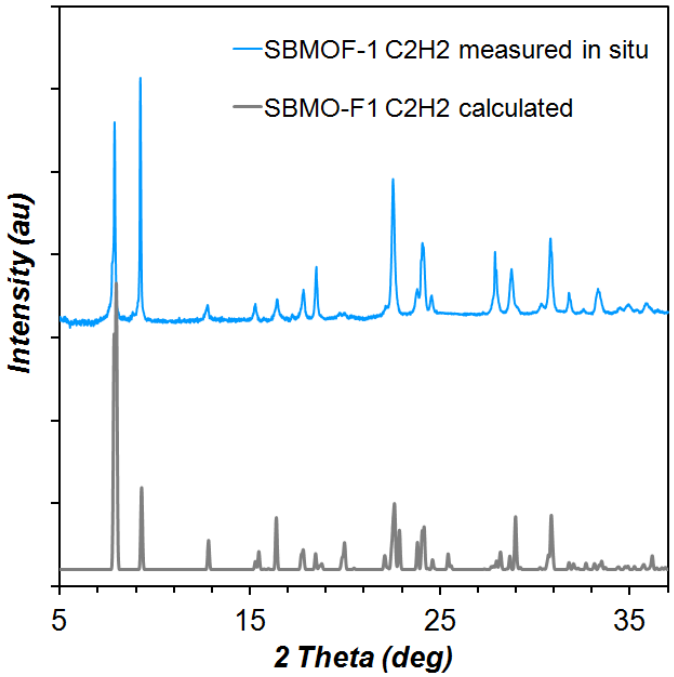

Figure S21. Calculated and measure in situ PXRD patterns of acetylene-loaded SBMOF-1.

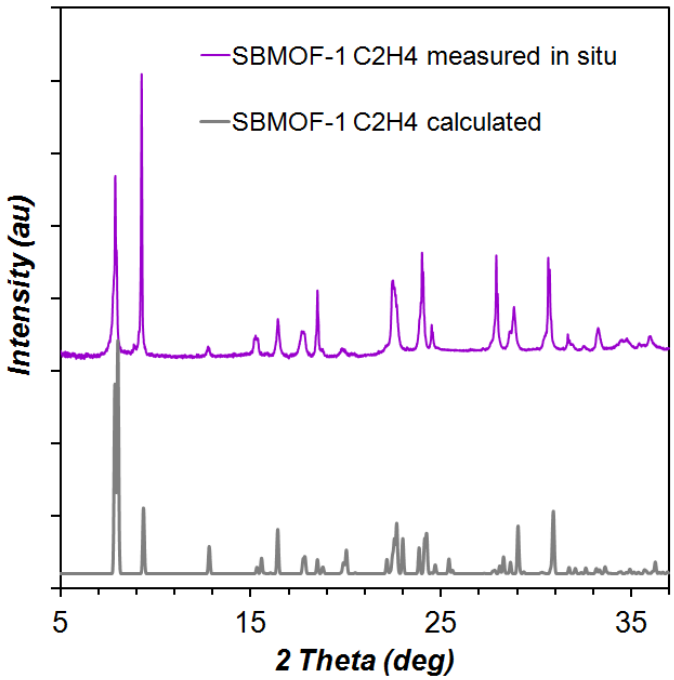

Figure S22. Calculated and measure in situ PXRD patterns of ethylene-loaded SBMOF-1.

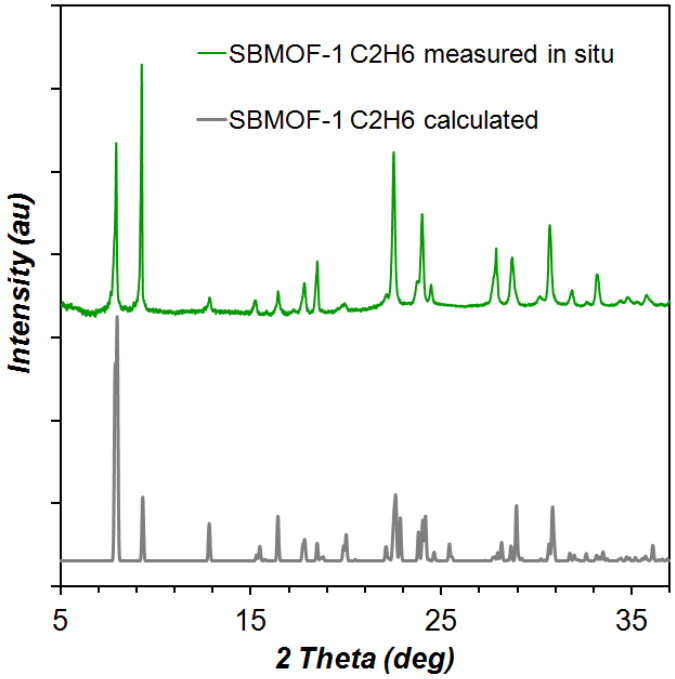

Figure S23. Calculated and measure in situ PXRD patterns of ethane-loaded SBMOF-1.

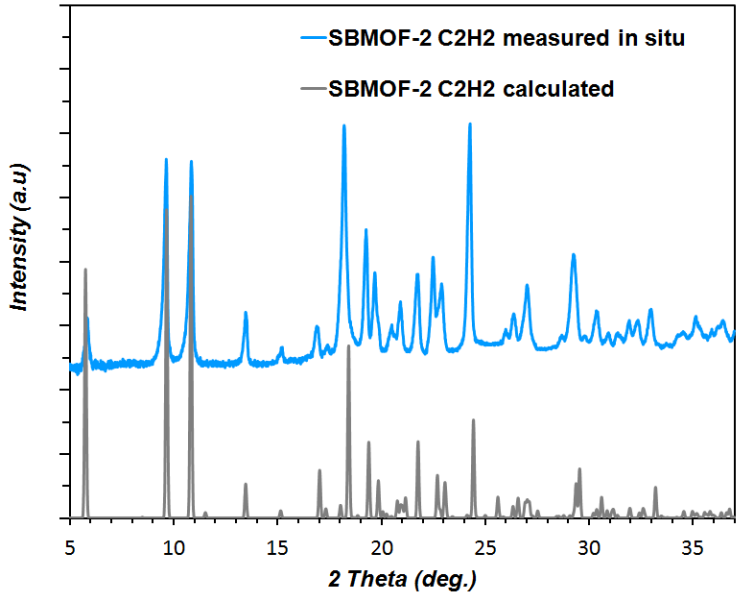

Figure S24. Calculated and measure in situ PXRD patterns of acetylene-loaded SBMOF-2.

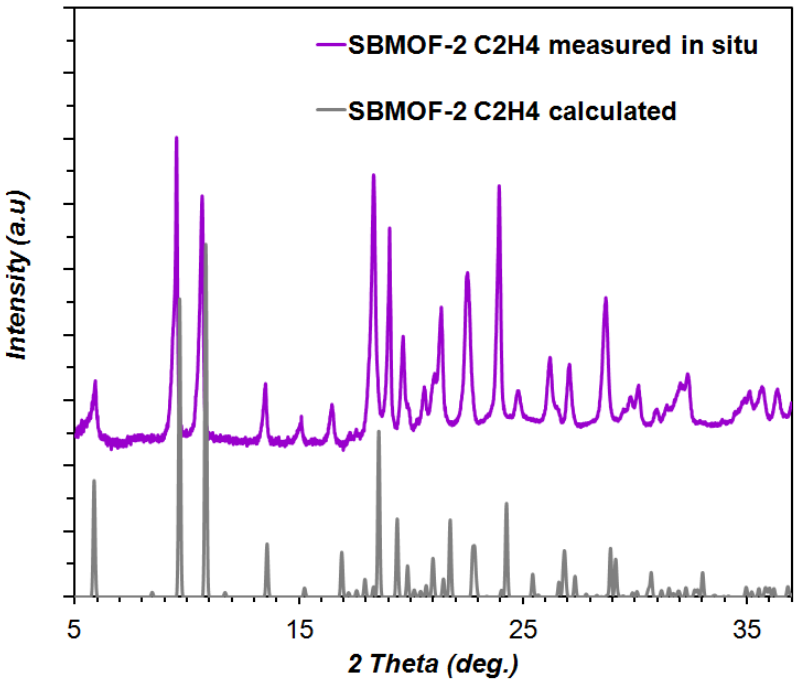

Figure S25. Calculated and measure in situ PXRD patterns of ethylene-loaded SBMOF-2.

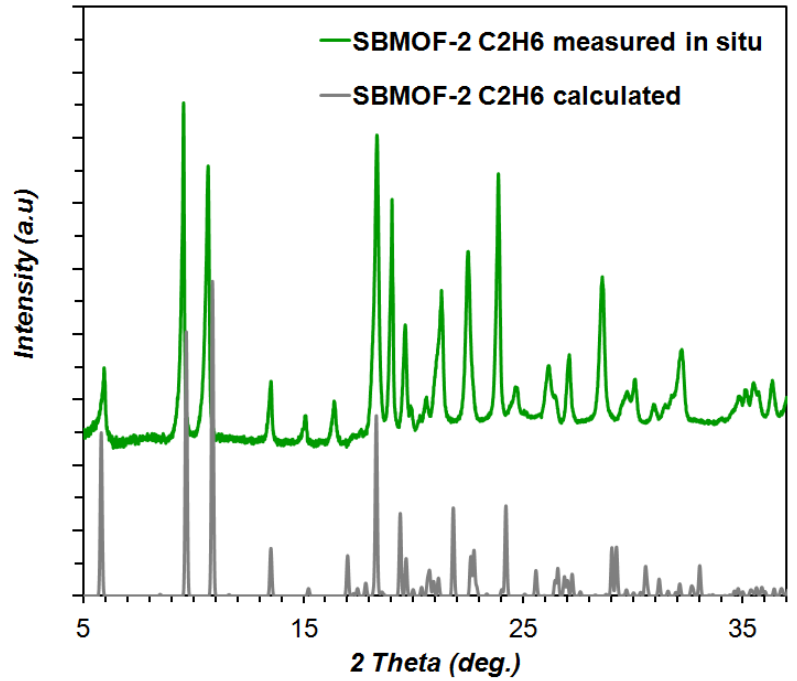

Figure S26. Calculated and measure in situ PXRD patterns of ethane-loaded SBMOF-2.

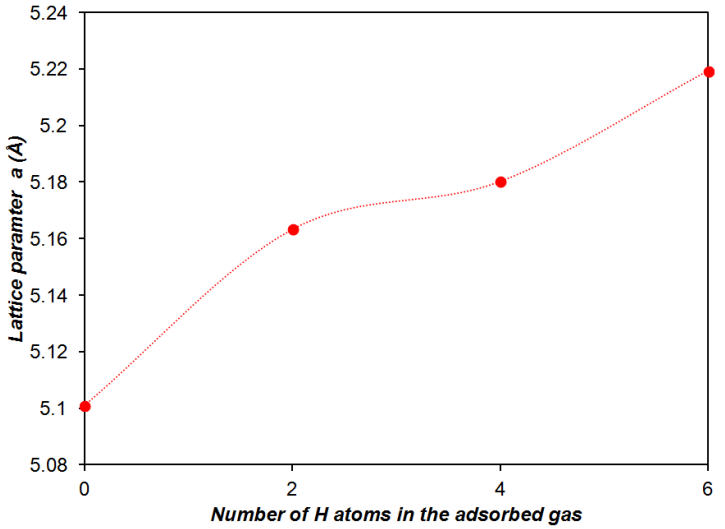

Figure S27. The development of the SBMOF-2 lattice parameter *a* with the size and number of H atoms of the adsorbed hydrocarbon gas. Line added to guide the eye.

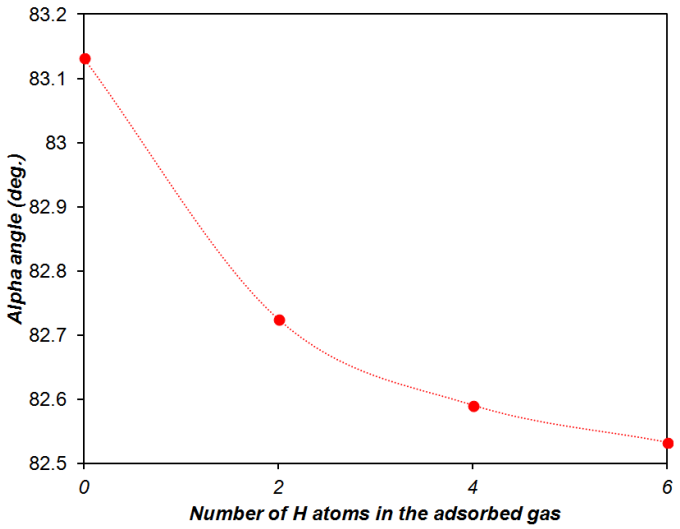

Figure S28. The development of the SBMOF-2 lattice angle α with the size and number of H atoms of the adsorbed hydrocarbon gas. Line added to guide the eye.

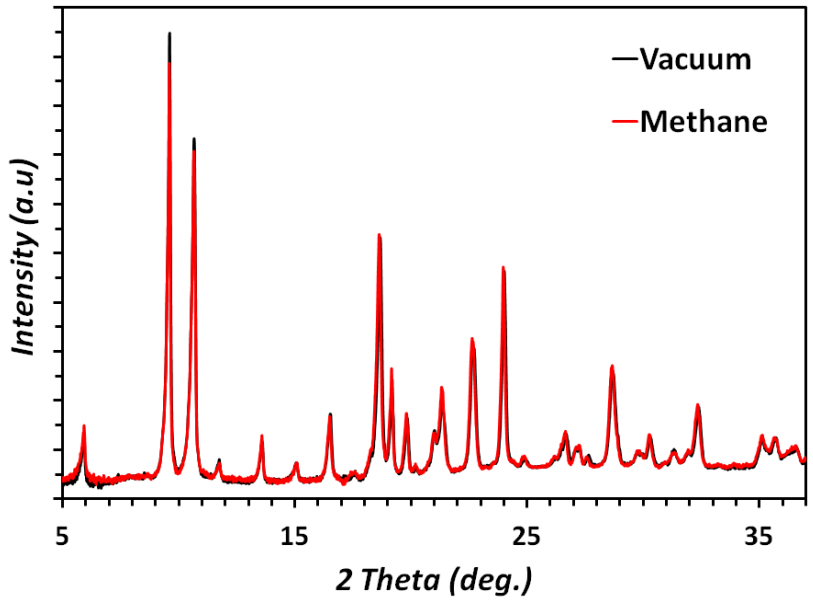

Figure S29. In situ PXRD patterns of activated and methane-loaded SBMOF-2.

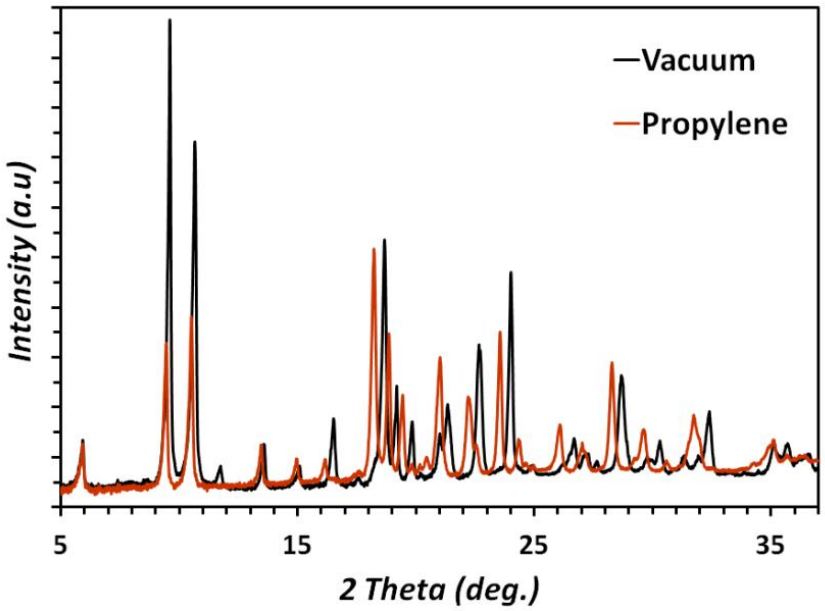

Figure S30. In situ PXRD patterns of activated and propylene-loaded SBMOF-2.

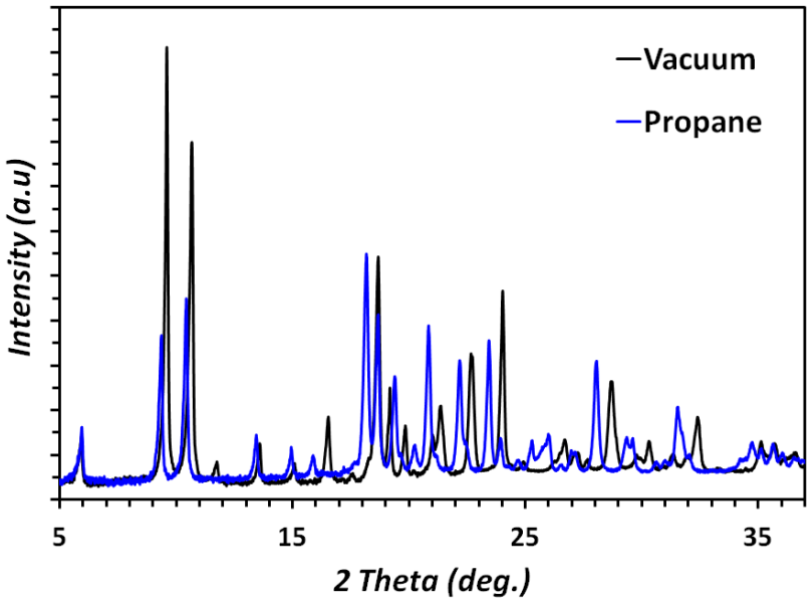

Figure S31. In situ PXRD patterns of activated and propane-loaded SBMOF-2.

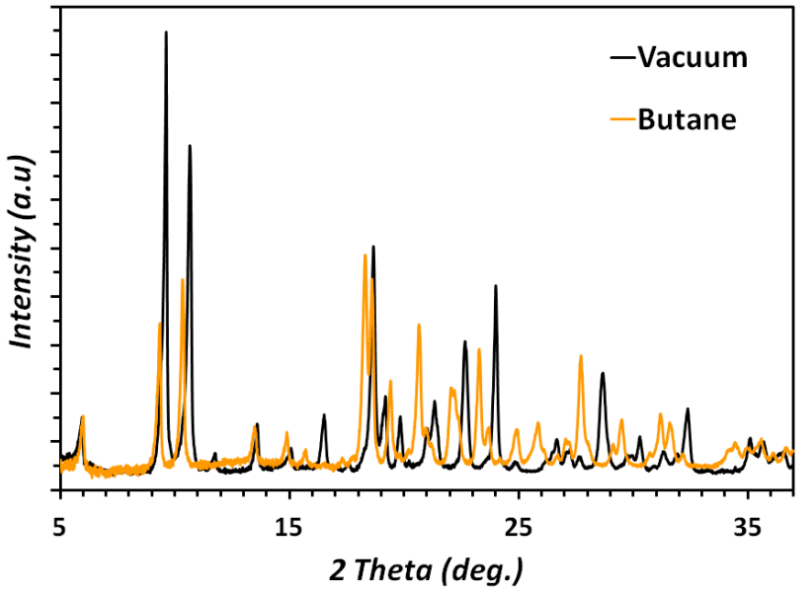

Figure S32. In situ PXRD patterns of activated and butane-loaded SBMOF-2.

Table S1. Parameters for DSLF isotherm fits

	N_1^{max} (mmol/g)	b_1 (1/kPa)	n_1	N_2^{max} (mmol/g)	b_2 (1/kPa)	n_2	R^2
CH_4@SBMOF-1	0.01000	0.8514	1.341	1.301	0.01235	1.079	0.9999
C_2H_2@SBMOF-1	0.6447	0.6250	1.093	0.7354	0.3849	1.009	0.9999
C_2H_4@SBMOF-1	1.208	1.404	1.100	0.1506	0.2509	0.8000	0.9999
C_2H_6@SBMOF-1	0.4712	5.347	1.677	0.8542	0.8077	0.9358	0.9999
CH_4@SBMOF-2	2.890	0.003496	1.012	8.01E-05	1.222	0.9900	0.9999
C_2H_2@SBMOF-2	2.959	0.02193	1.336	0.1951	0.5382	0.9857	0.9999
C_2H_4@SBMOF-2	2.805	0.03174	1.144	0.2703	0.2813	0.9629	0.9999
C_2H_6@SBMOF-2	2.524	0.08547	1.032	0.6190	0.06173	0.8900	0.9999

Table S2. Crystal data and structure refinement parameters for SBMOF-1:C_2H_n

Sample	**SBMOF-1:C_2H_2**	**SBMOF-1:C_2H_4**	**SBMOF-1:C_2H_6**
Empirical formula	$Ca(C_{14}H_8SO_6)\cdot(C_2H_2)_{0.35}$	$Ca(C_{14}H_8SO_6)\cdot(C_2H_4)_{0.34}$	$Ca(C_{14}H_8SO_6)\cdot(C_2H_6)_{0.43}$
Formula weight	353.33	353.88	357.27
T (K)	100(2)	100(2)	100(2)
Wavelength (Å)	1.54184	0.71073	0.41328
Space Group	$P2_1/n$	$P2_1/n$	$P2_1/n$
a (Å)	11.6583(3)	11.5955(3)	11.6667(11)
b (Å)	5.5671(1)	5.5581(1)	5.5586(5)
c (Å)	22.9110(6)	22.9548(5)	22.935(2)
α (°)	90	90	90
β (°)	100.901(2)	101.062(3)	101.011(3)
γ (°)	90	90	90
Volume ($Å^3$)	1460.16(6)	1451.93(6)	1460.0(2)
$Density_{calc}$ (g/cm^3)	1.607	1.619	1.625
Mu (mm^{-1})	5.320	0.604	0.144
Reflections, unique	9878	23013	9452
Reflections [$I>2\sigma(I)$]	3081	4416	2212
R_{int}	0.0341	0.0374	0.0639
Completeness to θ_{max}	0.992	0.998	0.888
F(000)	723.3	725.8	735.0
Goodness of fit	1.106	1.053	1.082
Data/restraints/parameter	3081/20/219	4416/18/213	2212/31/210
R_1[$I>2\sigma(I)$]	0.0446	0.0346	0.0998
wR_2 [all data]	0.1221	0.0905	0.2532

Table S3. Crystal data and structure refinement parameters for SBMOF-2:C_2H_n

Sample	**SBMOF-2:C_2H_2**	**SBMOF-2:C_2H_4**	**SBMOF-2:C_2H_6**
Empirical formula	$Ca(C_{34}H_{20}O_8)\cdot(C_2H_2)_{1.76}$	$Ca(C_{34}H_{20}O_8)\cdot(C_2H_4)_{1.47}$	$Ca(C_{34}H_{20}O_8)\cdot(C_2H_6)_{1.58}$
Formula weight	642.17	637.68	644.08
T (K)	100(2)	100(2)	100(2)
Wavelength (Å)	0.71073	1.54184	0.41328
Space Group	*P* -1	*P* -1	*P* -1
a (Å)	5.1634(2)	5.1803(3)	5.2195(2)
b (Å)	10.5518(5)	10.6508(5)	10.5691(5)
c (Å)	15.4849(7)	15.2914(6)	15.3604(7)
α (°)	82.725(4)	82.591(4)	82.533(1)
β (°)	87.233(4)	85.945(4)	86.657(1)
γ (°)	83.782(4)	82.739(4)	83.000(1)
Volume ($Å^3$)	831.44(6)	828.67(7)	833.14(6)
$Density_{calc}$ (g/cm^3)	1.283	1.278	1.284
Mu (mm^{-1})	0.240	2.060	0.067
Reflections, unique	24429	10168	4214
Reflections [$I>2\sigma(I)$]	4128	2888	2019
R_{int}	0.0643	0.0560	0.0213
Completeness to θ_{max}	0.993	0.953	0.710
F(000)	332.5	331.4	336.4
Goodness of fit	1.037	1.070	1.208
Data/restraints/parameter	4128/1/235	2888/ 11/ 221	2019/ 2/ 218
R_1[$I>2\sigma(I)$]	0.0464	0.0530	0.0384
wR_2 [all data]	0.1244	0.1260	0.1298

Table S4. Comparison of calculated and experimental enthalpies and heat of adsorption of C_2H_n in SBMOF-2 at 1 bar, 295 K.

HC Gas	ΔH (kJ/mol$_{MOF}$)			Q_{st} (kJ/mol$_{GAS}$)		
	Calculated		Experimental	Calculated		Experimental
	Virial	DSLF		Virial	DSLF	
CH_4	10.6	11.1	8.3(1)	23	24	18.0(2)
C_2H_2	53.1	62.3	55.4(4)	29	34	30.3(2)
C_2H_4	42.9	47.7	46.5(1)	27	30	29.2(1)
C_2H_6	52.9	56.2	53.5(1)	32	34	32.3(1)
C_3H_6	68.2	68.2	62.6(5)	43	43	39.5(3)
C_3H_8	69.1	65.9	62.8(3)	44	42	40.0(2)
C_4H_{10}	67.9	65.2	59.9(3)	50	48	44.1(2)

Table S5. Comparison of C_2H_n uptake values in SBMOF-1 and SBMOF-2 obtained trough isotherms measurments vs. crystal structure refinement results

	SBMOF-1		SBMOF-2	
	Gas occupancy (mol/mol)		Gas occupancy (mol/mol)	
	isotherms	refinement	isotherms	refinement
C_2H_2	0.46	0.35	1.72	1.76
C_2H_4	0.46	0.34	1.59	1.47
C_2H_6	0.45	0.43	1.65	1.58

References

1. Myers, A. L.; Prausnitz, J. M., Thermodynamics of Mixed-Gas Adsorption. *AIChE Journal* **1965,** *11*, 121-127.

2. Cessford, N. F.; Seaton, N. A.; Düren, T., Evaluation of Ideal Adsorbed Solution Theory as a Tool for the Design of Metal–Organic Framework Materials. *Ind. Eng. Chem. Res.* **2012,** *51*, 4911-4921.

3. Babarao, R.; Hu, Z.; Jiang, J.; Chempath, S.; Sandler, S. I., Storage and Separation of CO_2 and CH_4 in Silicalite, C168 Schwarzite, and IRMOF-1: a Comparative Study from Monte Carlo Simulation. *Langmuir* **2007,** *23*, 659-666.

4. Bae, Y.-S.; Mulfort, K. L.; Frost, H.; Ryan, P.; Punnathanam, S.; Broadbelt, L. J.; Hupp, J. T.; Snurr, R. Q., Separation of CO_2 From CH_4 Using Mixed-Ligand Metal-Organic Frameworks. *Langmuir* **2008,** *24*, 8592-8598.

5. Bae, Y.-S.; Farha, O. K.; Spokoyny, A. M.; Mirkin, C. A.; Hupp, J. T.; Snurr, R. Q., Carborane-Based Metal-Organic Frameworks as Highly Selective Sorbents for CO_2 Over Methane. *Chem. Commun.* **2008**, 4135-4137.

6. Zhang, Z.; Li, Z.; Li, J., Computational Study of Sdsorption and Separation of CO_2, CH_4, and N_2 by an rht-Type Metal-Organic Framework. *Langmuir* **2012,** *28*, 12122-12133.